

RD-A139 482

AN ACOUSTICAL IMAGING SYSTEM FOR THE INSPECTION OF
SOLID ROCKET MOTORS(U) BATTELLE PACIFIC NORTHWEST LAB
RICHLAND WA L J BUSSE ET AL JAN 84 AFRPL-TR-84-002

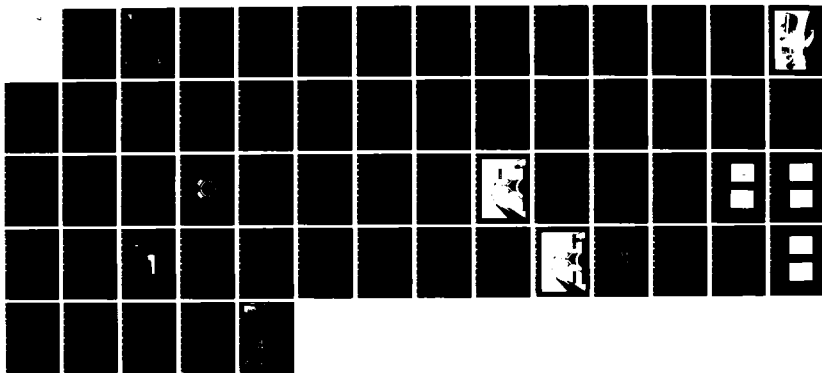
1/1

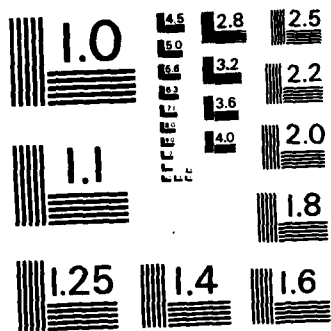
UNCLASSIFIED

F04611-81-C-0028

F/G 14/2

NL





MICROCOPY RESOLUTION TEST CHART
NATIONAL BUREAU OF STANDARDS - 1963-A

AD A1 39482



Final Report
for the period
July 1981 to
December 1983

AFRPL TR-84-002

AD:

131

An Acoustical Imaging System for the Inspection of Solid Rocket Motors

January 1984

Authors:
L. J. Busse
H. D. Collins
J. L. Eick
R. P. Gribble
P. D. Sperline

Battelle
Pacific Northwest Laboratories
Richmond, Washington 99352

F04611-81-C-0028

Approved for Public Release

Distribution unlimited. The AFRPL Technical Services Office has reviewed this report, and it is releasable to the National Technical Information Service, where it will be available to the general public, including foreign nationals.



prepared for the: Air Force
Rocket Propulsion
Laboratory

Air Force Space Technology Center
Space Division, Air Force Systems Command
Edwards Air Force Base,
California 93523

DTIC FILE COPY

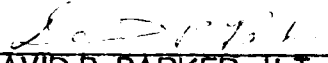
84 03 27 026

NOTICES

When U. S. Government drawings, specifications, or other data are used for any purpose other than a definitely related government procurement operation, the Government thereby incurs no responsibility nor any obligation whatsoever, and the fact that the Government may have formulated, furnished, or in any way supplied the said drawings, specifications, or other data, is not to be regarded by implication or otherwise, or conveying any rights of permission to manufacture, use, or sell any patented invention that may in any way be related thereto.

This report was submitted by Battelle Pacific Northwest Laboratories, Richland, Washington, 99352, under Contract F04611-81-C-0028, Job Order Number 573013 BA with the Air Force Rocket Propulsion Laboratory, Edwards AFB, CA 93523. The key technical personnel on this program were: Dr H. Dale Collins (Project Manager), Dr L. J. Busse (Deputy Manager), J. L. Eick, R. P. Gribble, and P. D. Sperline. This report has been reviewed, and is approved for publication.


PAT R. EMPLEO
Project Manager


DAVID P. PARKER, ILT, USAF
Chief, Structural Integrity Section

FOR THE DIRECTOR


EUGENE G. HABERMAN
Director, Solid Rocket Division

UNCLASSIFIED

SECURITY CLASSIFICATION OF THIS PAGE (When Data Entered)

REPORT DOCUMENTATION PAGE		READ INSTRUCTIONS BEFORE COMPLETING FORM
1. REPORT NUMBER AFRPL-TR-84-002	2. GOVT ACCESSION NO.	3. RECIPIENT'S CATALOG NUMBER
4. TITLE (and Subtitle) AN ACOUSTICAL IMAGING SYSTEM FOR THE INSPECTION OF SOLID ROCKET MOTORS Final Report		5. TYPE OF REPORT & PERIOD COVERED Final Report July 1981 to December 1983
		6. PERFORMING ORG. REPORT NUMBER
7. AUTHOR(s) L.J. Busse, H.D. Collins, J.L. Eick, R.P. Gribble, P.D. Sperline		8. CONTRACT OR GRANT NUMBER(s) F04611-81-C-0028
9. PERFORMING ORGANIZATION NAME AND ADDRESS Battelle Pacific Northwest Laboratories Richland, WA, 99352		10. PROGRAM ELEMENT, PROJECT, TASK AREA & WORK UNIT NUMBERS JON 573013 BA
11. CONTROLLING OFFICE NAME AND ADDRESS Air Force Rocket Propulsion Laboratory Edwards Air Force Base, CA, 93523		12. REPORT DATE January 1984
		13. NUMBER OF PAGES 64
14. MONITORING AGENCY NAME & ADDRESS(if different from Controlling Office)		15. SECURITY CLASS. (of this report) UNCLASSIFIED
		15a. DECLASSIFICATION DOWNGRADING SCHEDULE
16. DISTRIBUTION STATEMENT (of this Report) APPROVED FOR PUBLIC RELEASE; DISTRIBUTION UNLIMITED		
17. DISTRIBUTION STATEMENT (of the abstract entered in Block 20, if different from Report)		
18. SUPPLEMENTARY NOTES		
19. KEY WORDS (Continue on reverse side if necessary and identify by block number) Acoustic imaging, nondestructive testing, small solid rocket motors, inner-bore cracks, debonds, transmission test, chirp frequency ultrasonic test, desktop computer		
20. ABSTRACT (Continue on reverse side if necessary and identify by block number) This report describes the development and operation of an acoustical imaging, nondestructive test system for the inspection of small rocket motors. This system was built by Battelle, Pacific Northwest Laboratories for the U.S. Air Force Rocket Propulsion Laboratory at Edwards Air Force Base. This report is intended to document the accomplishments of the program, the theoretical background, and the operational characteristics of the inspection system. The major objective of this program was to develop an acoustical		

LEGAL NOTICE

This report was prepared by Battelle as an account of sponsored research activities. Neither Sponsor nor Battelle nor any person acting on behalf of either:

MAKES ANY WARRANTY OR REPRESENTATION, EXPRESS OR IMPLIED, with respect to the accuracy, completeness, or usefulness of the information contained in this report, or that the use of any information, apparatus, process, or composition disclosed in this report may not infringe privately owned rights; or

Assumes any liabilities with respect to the use of, or for damages resulting from the use of, any information, apparatus, process, or composition disclosed in this report.

1. Report title _____

2. Date _____

3. Type _____

4. Distribution _____

5. Justification _____

6. By _____

7. Distribution _____

8. Availability Codes _____

9. Avail and/or _____

Dist	Special
A-1	

TABLE OF CONTENTS

	<u>Page</u>
1.0 INTRODUCTION	1-1
1.1 OBJECTIVES	1-1
1.2 BACKGROUND	1-2
1.3 TEST SAMPLES	1-2
1.4 PROGRAM TASKS	1-3
1.5 SUMMARY AND CONCLUSIONS	1-3
2.0 THEORY OF INSTRUMENT OPERATION	2-1
2.1 DEBOND INSPECTION PROCEDURE	2-1
2.1.1 Input Impedance of a Single Layer System	2-1
2.1.2 Multiple Element Transmission Line	2-9
2.2 MEASUREMENT OF THE Q-SIGNATURE	2-11
2.3 MEASUREMENT OF THE R-SIGNATURE	2-13
2.4 MEASUREMENT OF INTERNAL DEFECTS	2-16
3.0 EXPERIMENTAL RESULTS IN INERT SIDEWINDER ROCKET MOTORS	3-1
3.1 DEBOND INSPECTION SYSTEM	3-1
3.1.1 Equipment Overview	3-3
3.1.2 Case/Liner Debond Results	3-7
3.1.3 Liner/Propellant Debond Results	3-11
3.2 INNER BORE CRACK INSPECTION SYSTEM	3-16
3.2.1 Equipment Overview	3-18
3.2.2 Inner Bore Crack Results	3-24
4.0 REFERENCES	4-1

LIST OF FIGURES

	<u>Page</u>
1.1 Photograph of Battelle/AFRPL Rocket Motor Inspection System	1-4
2.1 Illustration of the Waves Present in a Single Element Transmission Line	2-2
2.2 Input Impedance of a Single Element Transmission Line as a Function of Element Thickness (or equivalently; as a function of ultrasonic frequency)	2-7
2.3 Procedure for Calculating the Mechanical Input Impedance of a Multiple Element Transmission Line	2-10
2.4 Predicted "Q-signature" Response for a Sidewinder Rocket Motor Wall	2-12
2.5 Illustration of the Geometry Used to Measure the Reflection Coefficient of a Rocket Motor Wall	2-14
2.6 Predicted "R-signature" Response for a Sidewinder Rocket Motor Wall	2-15
2.7 Illustration of the Sound Propagation Path Used to Inspect for Internal Defects Within the Rocket Motor	2-17
3.1 Overall Block Diagram of the Rocket Motor Inspection System	3-2
3.2 Photograph Showing the Debond Test Transducer and Related Mechanical Assembly	3-4
3.3 Block Diagram of the Analog Electronics Used for the Debond Inspection	3-5
3.4A Photograph of the Monitor Display Oscilloscope when Inspection Frequency is Far From Mechanical Resonance of the Rocket Motor Wall	3-8

LIST OF FIGURES

(cont'd)

	<u>Page</u>
3.4B Photograph of the Monitor Display Oscilloscope When Inspection Frequency is at the Mechanical Resonance of the Rocket Motor Wall	3-8
3.5A Photograph of the Signature Display Oscilloscope Showing the "Q-signature" for a Case/Liner Debond	3-9
3.5B Photograph of the Signature Display Oscilloscope Showing the "R-signature" for a Case/Liner Debond	3-9
3.6A Results from a Series of "Q-signature" Measurements made in a Region of Case/Liner Debond	3-10
3.6B Results from a Series of "Q-signature" Measurements made in a Normal Region	3-10
3.7 Debond Defect Map Produced by the Rocket Motor Inspection System	3-12
3.8A Results from a Series of "Q-signature" Measurements made in a Region of Liner/Propellant Debond	3-13
3.8B Results from a Series of "R-signature" Measurements made in a Region of Liner/Propellant Debond	3-13
3.9A Results from a Series of "Q-signature" Measurements made in a Normal Region	3-14
3.9B Results from a Series of "R-signature" Measurements made in a Normal Region	3-14
3.10 Defect Map Produced by a Small Liner/Propellant Debond which had been Inserted Near the end of Rocket Motor	3-17
3.11 Photograph Showing Transducers and Test Head Assembly used for the Inner Bore Crack Test	3-19

LIST OF FIGURES

(cont'd)

	<u>Page</u>
3.12 Illustration of the Low Frequency Transducers which were Fabricated to Perform the Inner Bore Crack Test	3-20
3.13 Block Diagram of the Electronics used for the Inner Bore Crack Test	3-21
3.14A Photograph of the Monitor Oscilloscope Showing the Received Signal with No Defect Present	3-23
3.14B Photograph of the Monitor Oscilloscope Showing the Received Signal with a Defect Present	3-23
3.15 Defect Map Produced by a Naturally Occurring Inner Bore Crack	3-25

1.0 INTRODUCTION

This report describes the development and operation of an acoustical imaging, nondestructive test system for the inspection of small rocket motors. This system was built by Battelle, Pacific Northwest Laboratories for the U.S. Air Force Rocket Propulsion Laboratory at Edwards Air Force Base.

This report is intended to document the accomplishments of the program, the theoretical background, and the operational characteristics of the inspection system. In the remainder of this section, a review of the program objectives, background, samples, and results are presented. The theory of instrument operation is presented in Section 2. An overview of the electronic systems and results are presented in Section 3.

A detailed, step-by-step, operating procedure can be found in a separate document entitled, "Small Rocket Motor Inspection System - User's Manual/Programmer's Manual."

1.1 OBJECTIVES

The major objective of this program was to develop an acoustical imaging, nondestructive testing system for small rocket motors (i.e., 13-20 cm diameter). This inspection system was to be capable of detecting two types of defects within these rocket motors: 1) internal defects or inner-bore cracks, and 2) separations or debonds between the various layers making up the wall of the rocket motor.

After completion of the prototype, the system was to be delivered and demonstrated to Air Force personnel. This demonstration phase included the necessary training of AFRPL staff in the theoretical background and operating procedures for this inspection system.

1.2 BACKGROUND

This prototype and inspection system is based upon seven years of development and feasibility studies performed in the area of rocket motor inspection.(1-6) The first development work was performed upon large cylindrical sections from Minuteman rocket motors. This early study employed focused holographic detection for providing high resolution images of small inner bore radial cracks and case/liner/propellant debonds.

The emphasis for later work in acoustic inspection of solid rocket motors was redirected where the critical problem of detecting and imaging interface debonds existed. The spherical geometry, metal case thickness variations, and inner bore configurations (fin, star) increased the complexity of the inspection techniques. Two prototype inspection systems were developed to image debonds in the dome section: 1) variable or chirp frequency system, and 2) low frequency transmission system.

The present laboratory prototype makes use of both of these techniques to detect debond and inner bore cracks on small rocket motors.

1.3 TEST SAMPLES

Three test specimens were provided by the U.S. Air Force for development and evaluation of the laboratory prototype system. Two of these samples were inert "Sidewinder" training motors which were loaded with simulated (i.e., non-activated) propellant. These two training motors were manufactured by Thiokol and had steel cases. One of these motors was sectioned during the course of the program to make a number of smaller test pieces. These pieces were used to simulate a variety of debond and inner bore crack conditions. The third sample was a "Sidewinder" manufactured by Aerojet which had previously been test fired and subsequently relined. This sample was made of a light alloy

(such as aluminum) and was used to assess the difficulty of inspecting through different materials and different internal sample geometry.

1.4 PROGRAM TASKS

The program consisted of essentially two phases:

- 1) Design, construction, and evaluation of the prototype solid rocket motor inspection system.
- 2) Demonstration and training of U.S. Air Force Rocket Propulsion Laboratory personnel on the ¹ cry and use of the inspection system.

1.5 SUMMARY AND CONCLUSIONS

An experimental, or laboratory, prototype system for the inspection of solid rocket motors has been built, tested, and made operational at Edwards Air Force Base. Figure 1.1 shows the completed imaging/inspection system. This system is capable of handling rocket motors as large as 80 inches in length, 11 inches outside diameter, and up to 500 pounds.

The device is capable of performing two types of ultrasonic tests upon small solid rocket motors: 1) a chirp frequency ultrasonic test for detection of debonds or separation of layers in the wall of the rocket motor, and 2) a low frequency transmission test for detection of defects within the solid rocket motors. The data collection system is controlled by the operator through a small desktop computer. This computer relieves the operator of performing repetitive setup and calibration functions and also is used to predict and classify the ultrasonic response of the rocket motors.

The performance tests and training of Air Force personnel on the use of this laboratory system were performed using inert Sidewinder rocket motors. With this test specimen, the system

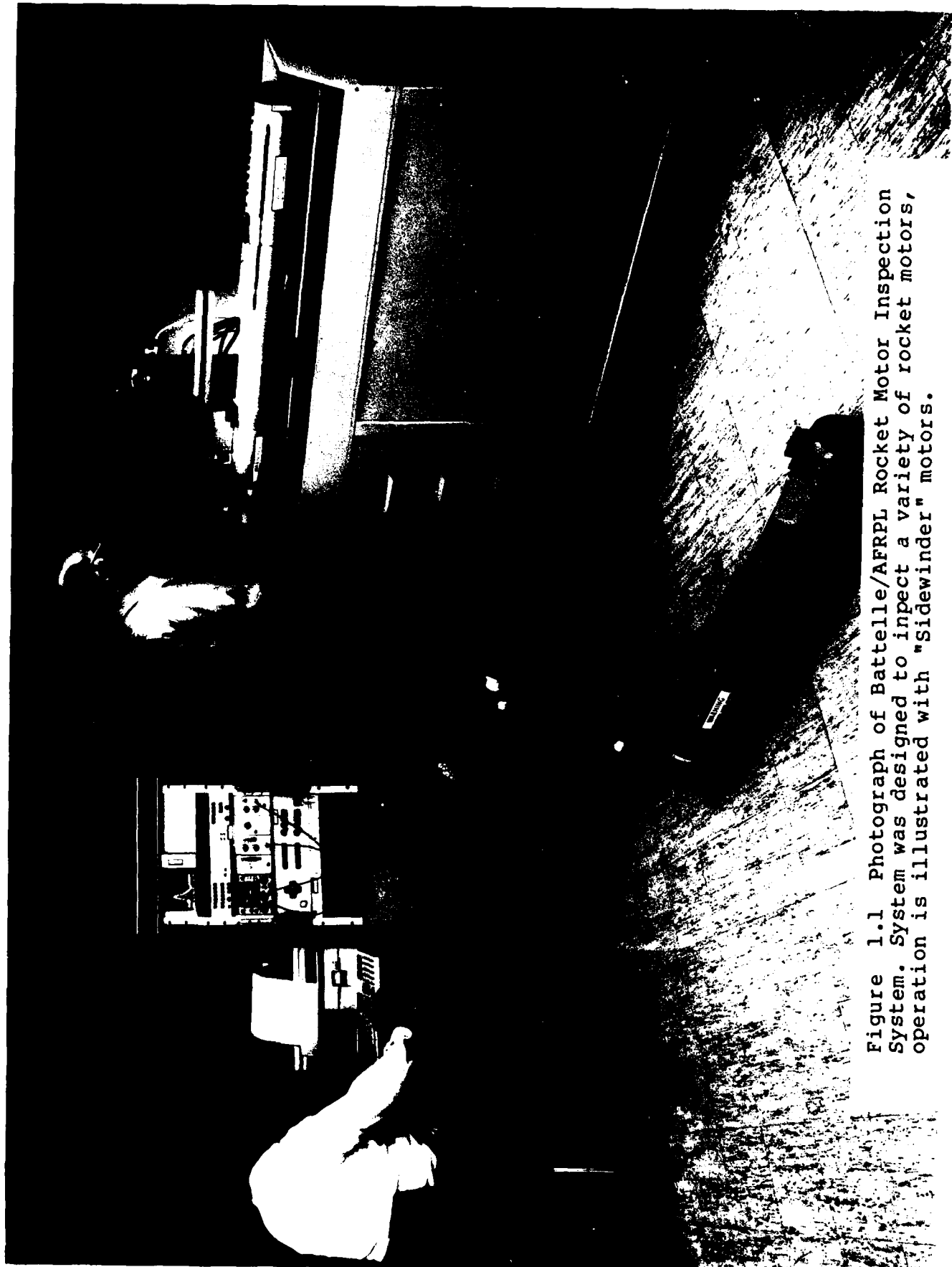


Figure 1.1 Photograph of Battelle/AFRPL Rocket Motor Inspection System. System was designed to inspect a variety of rocket motors, operation is illustrated with "Sidewinder" motors.

was shown to be capable of detecting all of the flaw types it was originally designed to detect:

- 1) Case/Liner Debonds
- 2) Liner/Propellant Debonds
- 3) Inner-Bore Cracks

Case/liner debonds are reliably detected using the chirp frequency debond test, and the other two flaw types are evident using the low frequency transmission test. This test system is expected to be applied to the following types of "live" motors:

- Sidewinder
- Maverick
- Sparrow
- Harm
- Shrike

Use of this test system by Air Force personnel will allow the condition of these small rocket motors to be assessed and will hopefully contribute to improved performance and safety procedures.

2. ^ THEORY OF INSTRUMENT OPERATION

The acoustical imaging, nondestructive testing system for small rocket motors was designed to perform two different tests: 1) test for separation or debonds between the layers which make up the rocket motor wall, and 2) test for internal defects within the propellant or "inner bore" cracks. The physical setup for these two different tests, as well as the theory behind these two tests, is different. In this section of the report, the theory for these tests is presented along with some sample calculations for simple structures.

2.1 DEBOND INSPECTION PROCEDURE

A debond by definition is a discontinuity or separation between layers which make up a layered, composite structure. These separations can be thought of as very thin air gaps or voids in the layered structure. These gaps will change the physical properties of the layered structure, and this change is related to the way the layered structure resonates when it is excited by an ultrasonic pulse. In this section, the theory of layered resonant structures is presented.

An analytical model is used to predict these resonant properties in terms of the "Q" or quality factor of the resonance and in terms of the reflectivity of the layered structure. This model makes use of the mechanical input impedance of the layered structure to calculate Q and reflection coefficients. Computer generated signatures (based on "Q" or "Reflection Coefficient") are then analyzed to determine the type of debond and the frequency range for making the chirp frequency measurements.

2.1.1 Input Impedance of a Single Layer System

A diagram of a single layer system or ultrasonic transmission line is given in Figure 2.1. The origination medium is

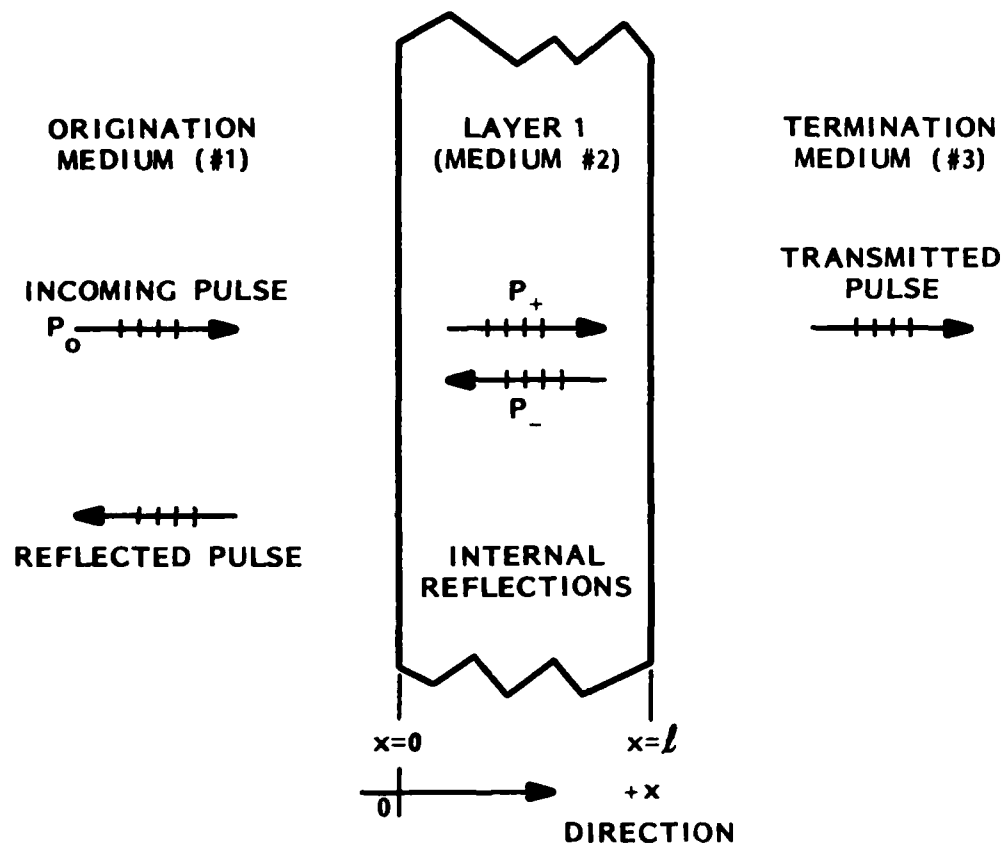


Figure 2.1 Illustration of the waves present in a single element transmission line.

the material in which the ultrasonic plane wave, P_0 , originates. (For immersion testing, this medium is the water bath.) It is assumed to be infinitely thick relative to medium 2. In practice, this is achieved by having a transmission path long enough that no multiple echoes in medium 1 occur while the measurement is being made. The first layer (second medium) has a finite thickness and supports ultrasonic waves traveling in both the forward (+X) and backward (-X) directions. These waves are designated as P_+ and P_- respectively. The sum of the two waves is P_2 . The final or terminating medium is also thick enough that no echoes from its back surface reach the interface to layer 1 during the measurement period. Hence medium 3 has only one wave P_3 and it travels in the +X direction. Each of the three media has a density, ρ , velocity, v , and attenuation coefficient, α .

The temporal and spatial dependence of the nth pressure wave can be expressed as

$$P_n(X) = P_n e^{i\omega t} e^{-\theta_n X} \quad (1)$$

where the complex propagation parameter θ_n is

$$\theta_n = \alpha_n + i\omega/v_n. \quad (2)$$

The frequency of the wave, f , the angular frequency, ω , and the wavelength, λ , are related by the general equations

$$\omega = 2\pi f \quad (3)$$

$$\text{and } v_n = f\lambda_n. \quad (4)$$

The general wave equation for a volume element experiencing a pressure, p , and displacement from equilibrium, ξ , is(7)

$$\frac{-\partial p_n(x,t)}{\partial x} = \rho_n \frac{\partial^2 \xi_n(x,t)}{\partial t^2} \quad (5)$$

Since the particle displacement will be sinusoidal in time,

$$\frac{\partial^2 \xi}{\partial t^2} = \frac{\partial^2}{\partial t^2} (\xi_0 e^{i\omega t}) = i\omega \frac{\partial \xi}{\partial t} . \quad (6)$$

Since the velocity

$$U(x) = \frac{\partial \xi(x)}{\partial t} ,$$

then Equation (5) becomes

$$\frac{+\partial p_n(x)}{\partial x} = -i\omega \rho_n U_n(x) \quad (7)$$

The specific acoustic impedance, Z , of a material is defined as the complex ratio of the sound pressure to the particle velocity(7), i.e.,

$$Z(x) = \frac{P(x)}{U(x)} . \quad (8)$$

To obtain the impedance of layer 1, we first calculate the quantity $U_2(x)$. The sound pressure $P_2(x)$ is the sum of $P_+(x)$ and $P_-(x)$; hence

$$P_2(x) = P_+ e^{-\theta_2 x} + P_- e^{+\theta_2 x} \quad (9)$$

where the time dependence $e^{i\omega t}$ has been suppressed. Using equation (7), we obtain

$$U_2(x) = \frac{-1}{i\omega \rho_2} \frac{\partial P_2(x)}{\partial x}$$

$$\text{giving } U_2(X) = \frac{\theta_2}{i\omega\rho_2} [P_+e^{-\theta_2 X} - P_-e^{+\theta_2 X}] \quad (10)$$

Using the definition in Equation (8), the impedance is obtained by dividing Equation (9) by Equation (10) to obtain

$$Z_2(X) = \frac{i\omega\rho_2}{\theta_2} \left[\frac{P_+e^{-\theta_2 X} + P_-e^{+\theta_2 X}}{P_+e^{-\theta_2 X} - P_-e^{+\theta_2 X}} \right] \quad (11)$$

The "characteristic impedance" of medium 2 is denoted by Z_{02} and is defined as the quantity

$$Z_{02} = \frac{i\omega\rho_2}{\theta_2} = \frac{i\omega\rho_2}{\alpha + i\omega/v_2}. \quad (12)$$

This can be rearranged to be

$$Z_{02} = \frac{i\rho_2 v_2}{i + \frac{\alpha v}{\omega}} \quad (13)$$

In most situations, the quantity $\frac{\alpha v}{\omega} \ll 1$, so the characteristic impedance is just the density times the velocity, i.e.,

$$Z_{02} = \rho_2 v_2. \quad (14)$$

Using Equation (14), Equation (11) becomes

$$Z_2(X) = Z_{02} \left[\frac{P_+e^{-\theta_2 X} + P_-e^{+\theta_2 X}}{P_+e^{-\theta_2 X} - P_-e^{+\theta_2 X}} \right]. \quad (15)$$

At the boundaries of layer 1 ($X=0$ and $X=+\ell$), the specific acoustic impedances are

$$Z_2(0) = Z_{02} \left[\frac{P_+ + P_-}{P_+ - P_-} \right] \quad (16)$$

$$\text{and } Z_2(\ell) = Z_{02} \left[\frac{P_+ e^{-\theta_2 \ell} + P_- e^{+\theta_2 \ell}}{P_+ e^{-\theta_2 \ell} - P_- e^{+\theta_2 \ell}} \right]. \quad (17)$$

The variables P_+ and P_- can be eliminated from these equations to give

$$Z_2(o) = Z_{02} \left[\frac{Z_2(\ell) + Z_{02} \tanh(\theta_2 \ell)}{Z_{02} + Z_2(\ell) \tanh(\theta_2 \ell)} \right]. \quad (18)$$

Since particle velocity and pressure must be continuous across the boundary at $Z = \ell$, it follows that $Z_2(\ell) = Z_{03}$, where Z_{03} is the characteristic impedance of medium 3. Since medium 3 is infinite, its impedance at $X = \ell$ will be just its characteristic impedance. Hence Equation (18) reduces to

$$Z_2(o) = Z_{02} \left[\frac{Z_{03} + Z_{02} \tanh(\theta_2 \ell)}{Z_{02} + Z_{03} \tanh(\theta_2 \ell)} \right]. \quad (19)$$

The quantity $Z_2(o)$ is called the input impedance of medium 2. $Z_2(o)$ is also dependent on the thickness, attenuation, and velocity of medium 2 and the frequency of the ultrasonic wave.

Rewriting this equation in simpler notation,

$$Z_{in} = Z_0 = \frac{Z_{term} + Z_0 \tanh \tilde{\theta} \ell}{Z_0 + Z_{term} \tanh \tilde{\theta} \ell} \quad (20)$$

where Z_{in} , Z_{term} , and Z_0 are the input, terminating, and characteristic impedance of the line, respectively. This equation holds for any single element transmission line.

Figure 2.2 shows an example of the input impedance of a single element transmission line for two different extremes of loading or terminating impedance. The line is assumed to be made of a material such as aluminum ($Z_0 = 17 \times 10^5$ Rayls) and is assumed to be 0.125 in. (3.18 mm) thick. The input impedance is plotted as a function of ultrasonic frequency or equivalently in terms of the layer thickness expressed in wavelengths.

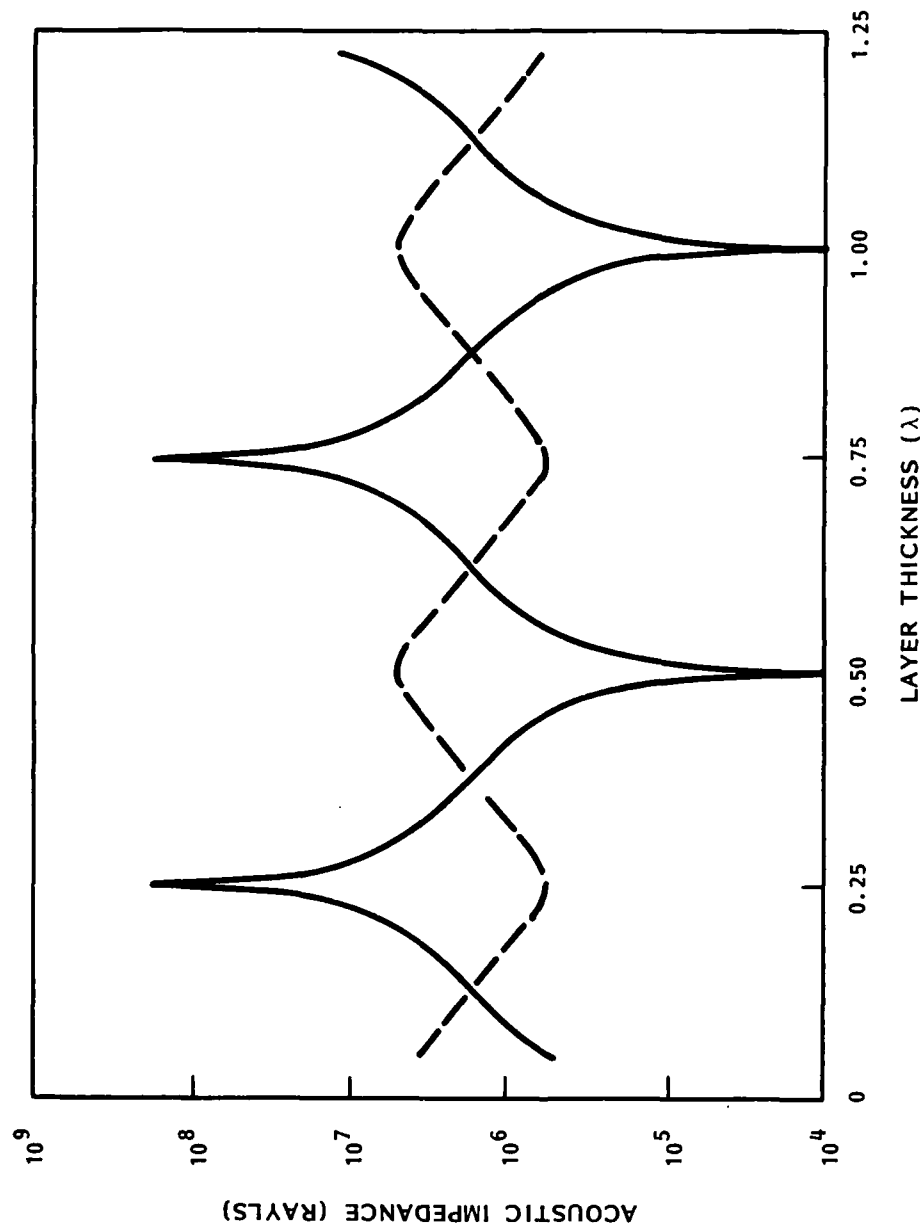


Figure 2.2 Input impedance of a single element transmission line as a function of element thickness (or equivalently; as a function of ultrasonic frequency). Solid line shows response for light mechanical load and dashed line shows response for heavy mechanical load.

The solid lines show the resonant properties of the line when it is backed or terminated with a low impedance material such as air. Under these conditions ($Z_{term} \ll Z_0$), Equation (20) reduces to

$$Z_{in} = Z_0 \tanh \tilde{\theta}l. \quad (21)$$

For a low loss material such as aluminum ($\alpha \ll \omega/v$), this equation reduces further to

$$Z_{in} = i\rho_c \tan \frac{\omega l}{v}. \quad (22)$$

The line is resonant (impedance minima) whenever

$$\frac{\omega l}{v} = n\pi \quad n = 0, 1, 2, 3 \dots \quad (23)$$

or when

$$l = n\frac{\lambda}{2} \quad (24)$$

The line thickness is equal to an integer number of half wavelengths.

The dashed curve shows how the resonant properties of the line change as the impedance of the backing material is increased. The curve illustrates the resonant properties of the aluminum transmission line backed with a high impedance material such as steel ($Z_0 = 50 \times 10^5$ Rayls). Under these conditions ($Z_{term} \ll Z_0$), Equation (11) reduces to

$$Z_{in} = ilc \cot \frac{\omega l}{v} \quad (25)$$

The line is resonant whenever

$$\frac{\omega l}{v} = n \frac{\pi}{2} \quad n = 1, 3, 5, \dots \quad (26)$$

or when

$$l = n \frac{\lambda}{4} \quad n = 1, 3, 5, \dots \quad (27)$$

The thickness is equal to an odd number of quarter wavelengths.

2.1.2 Multiple Element Transmission Line

The theory for the input impedance of a single element transmission line can be extended to multiple element transmission lines in a straight forward manner. The procedure is illustrated in Figure 2.3. In panel A, an n -element transmission line is shown. Each element has propagation parameters θ_n and length l_n . To calculate the total input impedance of the line, the single element equation must be applied n times. Panel B shows the first calculations. It is identical to the calculation for a single element transmission line

$$Z_{in1} = Z_{o1} \left[\frac{Z_{term} + Z_{o1} \tanh \theta_1 l_1}{Z_{o1} + Z_{term} \tanh \theta_1 l_1} \right] \quad (28)$$

This calculated impedance looking into element 1 now becomes the terminating impedance for element 2, as is illustrated in panel C.

$$Z_{in2} = Z_{o2} \left[\frac{Z_{in1} + Z_{o2} \tanh \theta_2 l_2}{Z_{o2} + Z_{in2} \tanh \theta_2 l_2} \right] \quad (29)$$

This procedure is applied sequentially until the last element in the transmission line is reached.

This procedure for calculating the input impedance of a multiple element transmission line is best suited for numerical analysis on a computer where an iterative procedure for calculating Z can be set up. A computer program was written for this

MULTI-ELEMENT TRANSMISSION LINE

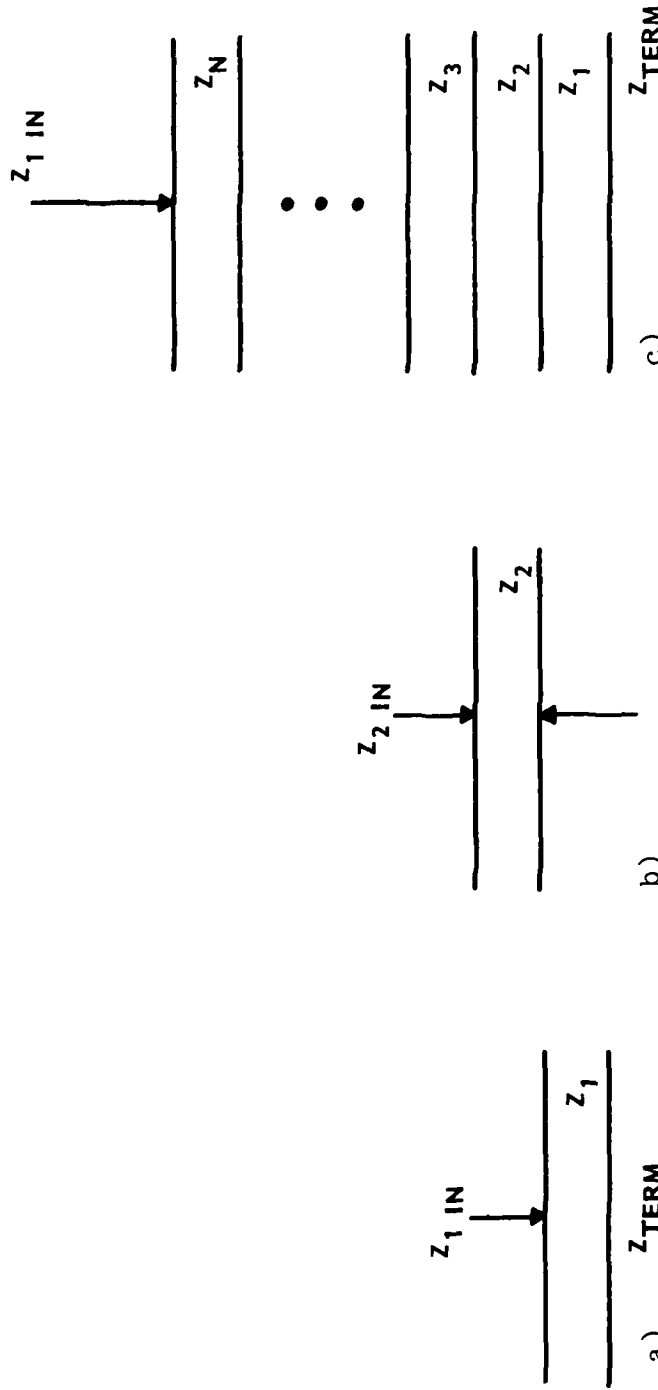


Figure 2.3 Procedure for calculating the mechanical input impedance of a multiple element transmission line.

purpose and is discussed in the User/Programmer's Manual. Results are discussed later in this report for calculating the frequency dependence of the reflection coefficient and the Q of a multielement transmission line.

2.2 MEASUREMENT OF THE Q-SIGNATURE

It is difficult to measure the input impedance of a multi-layer transmission line directly. The impedance, however, does control the resonant properties of the line and changes in impedance can be inferred from changes in the quality factor or the acoustic response of the composite resonator.

For a resonant structure, the Q is usually defined as the ratio stored in the resonant structure to the energy dissipated in the structure. Another way to quantify the response of a layered structure is in terms of the acoustic response.

The acoustic response of the multilayer transmission line is determined by the acoustic impedances of the transducer used to make the measurement Z_T , the effective transducer backing, Z_B , and the input impedance Z_{in} . The Q of this system⁽⁸⁾ is given by

$$Q \propto \frac{Z_T}{Z_B + Z_{in}}. \quad (30)$$

Figure 2.4 shows the acoustic response or quality factor for the Sidewinder rocket motor structure (steel case 0.057 in. thick, rubber liner 0.05 in. thick, and propellant). The dashed line represents the acoustic response when all layers of the rocket motor are tightly bonded. The dotted line indicates the response when a debond is present between liner and propellant, and the solid line shows the predicted response when a debond is present between case and liner. The effective backing impedance of 3.0×10^3 Rayls was chosen so that these predictions would be in agreement with the experimental data.

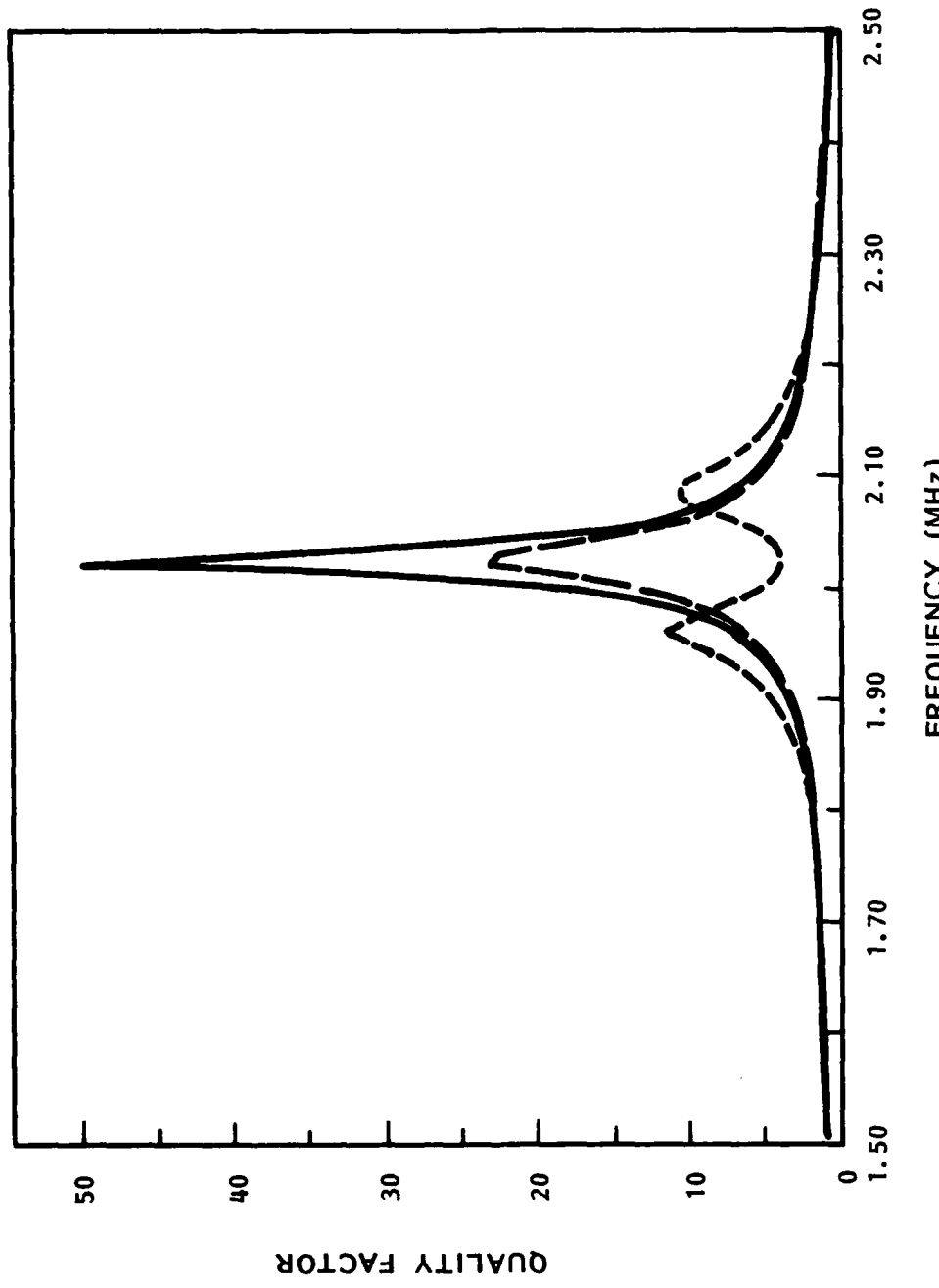


Figure 2.4 Predicted "Q-signature" responses for a Sidewinder rocket motor wall. Solid line shows Case/Liner debond, long dashed line shows Normal response and short dashed line shows predicted Liner/Propellant debond response.

2.3 MEASUREMENT OF THE R-SIGNATURE

The input impedance of a multilayer transmission line also effects the way ultrasonic energy is reflected from the line. For normal incidence from a plane surface, the reflection coefficient of the surface can be written as:

$$R = \frac{Z_W - Z_{in}}{Z_W + Z_{in}} \quad (31)$$

where Z_W is the impedance of the material in which the incident energy is propagating and Z_{in} is the input impedance looking into the surface. For the conditions shown in Figure 2.5, the reflection coefficient is independent of the transducer dimensions so long as Z_{in} is uniform over the extent of the ultrasonic beam. If the incident pulse is traveling in an extended medium such as water where the spatial length of the pulse ℓ is less than the distance d , no standing waves will be observed in the water and all of the frequency dependence observed in the reflected signal will be caused by the frequency dependence of the input impedance Z_{in} .

Figure 2.6 shows three different reflection signatures for the Sidewinder motor wall structure. For the normal condition where all layers of the motor wall are tightly bonded, a slight dip in the reflection coefficient is predicted and the frequency of this dip is largely controlled by the resonant properties of the steel case. When a case-liner debond exists, a larger dip in the reflected signal is predicted. The reflected signal predicted for the liner-propellant debond condition is the most interesting because the effects of two resonant layers are observable. The details of this double dip structure, however, is quite sensitive to the exact thickness of the liner layer.

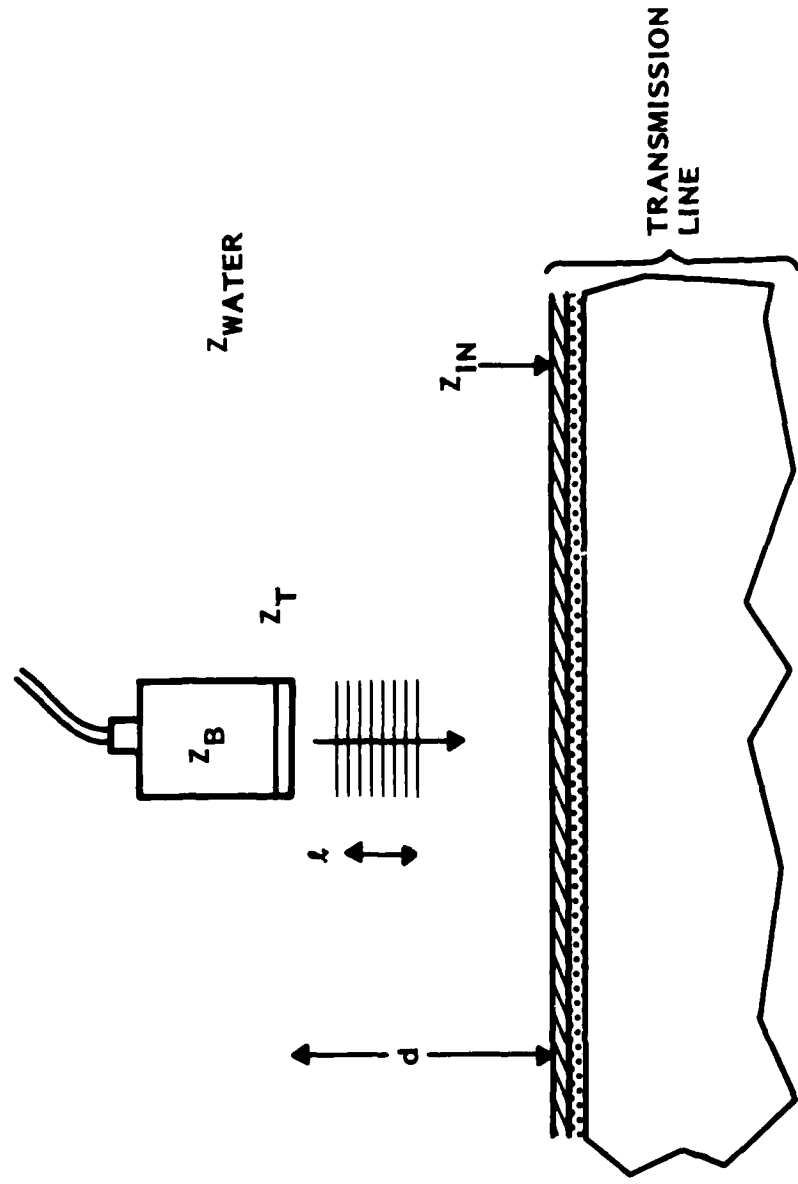


Figure 2.5 Illustration of the geometry used to measure the reflection coefficient of a rocket motor wall. Same set-up is used to measure the "Q-signature" response.

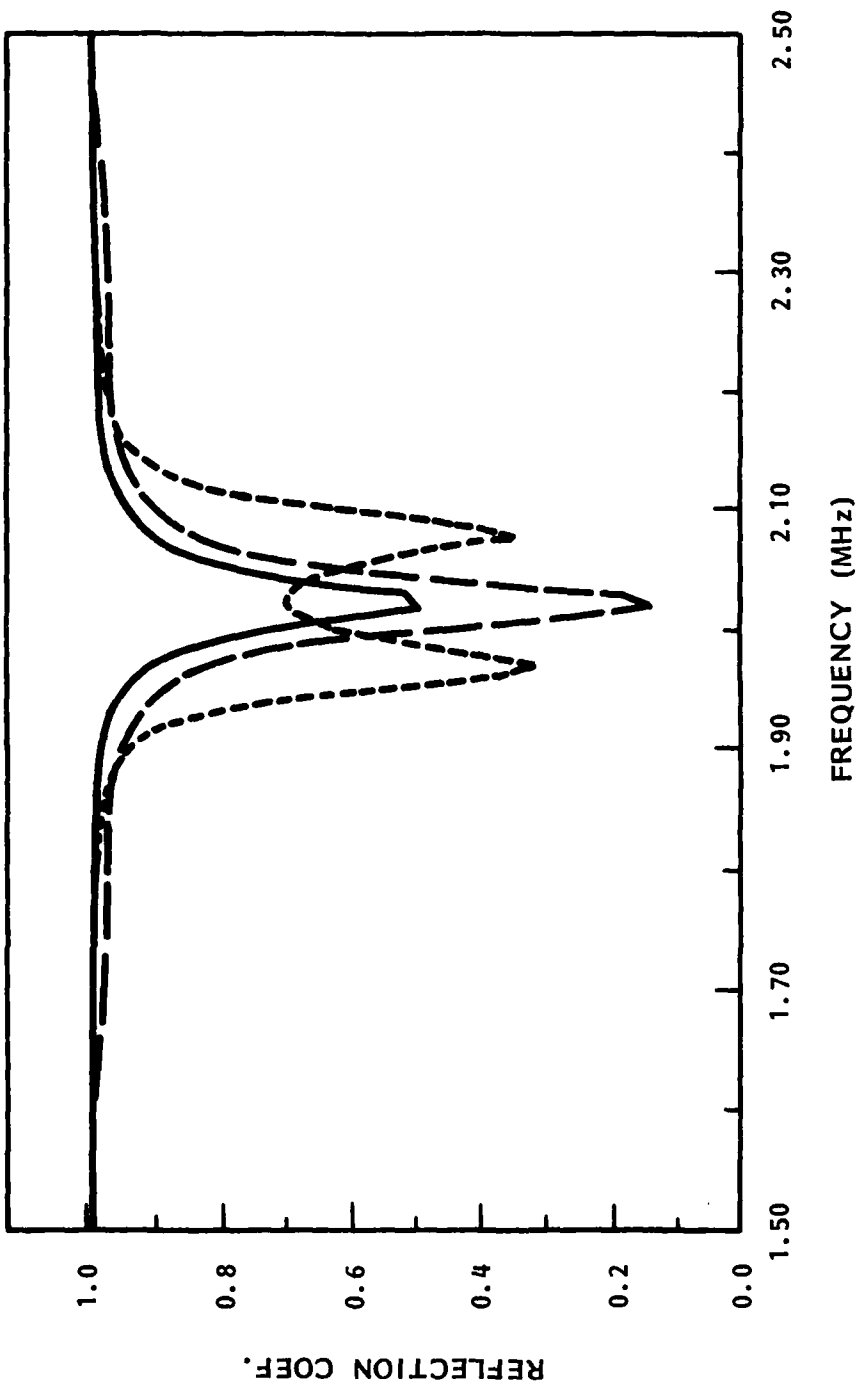


Figure 2.6 Predicted "R-signature" responses for a Sidewinder rocket motor wall. Solid line shows Case/Liner debond, long dashed line shows Normal response and short dashed line shows predicted Liner/Propellant debond response.

2.4 MEASUREMENT OF INTERNAL DEFECTS

In order to detect internal defects within the small rocket motors, a transmission test is also performed. Figure 2.7 illustrates the geometry associated with this test. A pulse of ultrasonic energy is launched from the transmitting transducer, propagates through the rocket motor wall, is reflected from the inner bore of the rocket motor, and propagates to the receiving transducer. This test is performed at a low frequency of 58 kHz using a long gated burst of ultrasonic energy. This low frequency was chosen to provide adequate penetration through the highly attenuative propellant material.

Under normal circumstances (bonded layers in motor wall and no inner bore cracks), an ultrasonic pulse is transmitted through the motor wall and received by the receiving transducer. This pulse can be blocked however by:

- 1) Inner bore cracks, or
- 2) Debonded layers under transmitter or receiver.

As the transmitter-receiver are scanned over the motor wall, a defect condition is recorded when the amplitude of the transmitted ultrasonic pulse falls below a predetermined level. The type of defect must be inferred from the image or the pattern which is recorded during the scanning procedure:

- Inner bore cracks will appear as single indications. The length and angular extent of the indication is determined by the length and depth of the crack, respectively.
- Debonded regions will appear as double indications; the signal is blocked when the debond is under the transmitter and the receiver. The length and angular extent of the individual indications is determined by the size of the debonded region. The angular separation of the two indications is fixed and is equal to

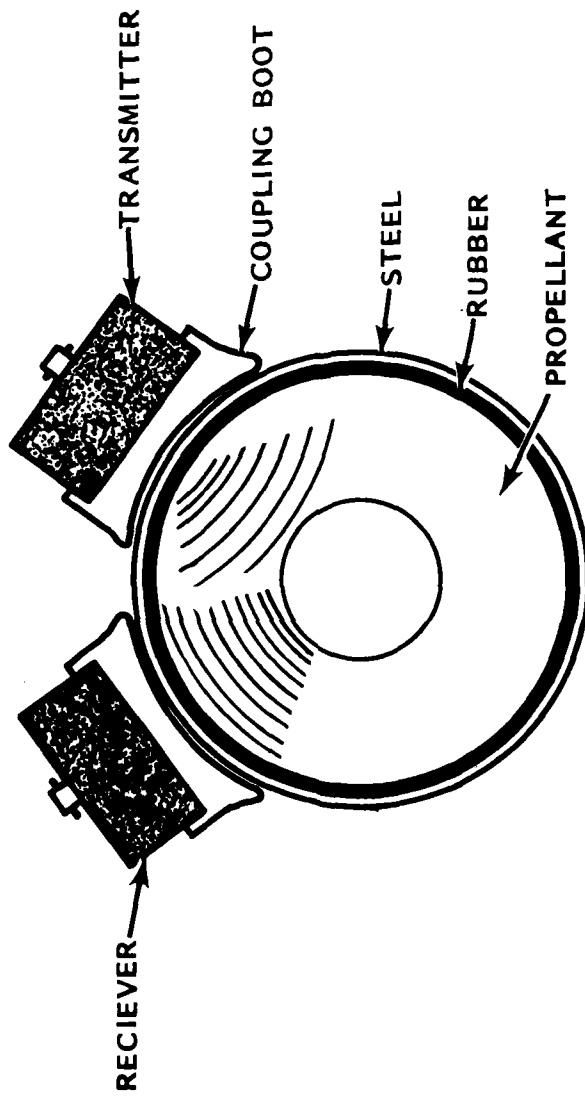


Figure 2.7 Illustration of the sound propagation path used to inspect for internal defects within the rocket motors.

the angular separation of the transmitter and receiver pair.

In Section 3 of this report, examples are provided of the types of images which are produced using this low frequency transmission testing technique.

3.0 EXPERIMENTAL RESULTS ON INERT SIDEWINDER ROCKET MOTORS

In this section, the experimental procedures for detecting debonds and inner bore cracks on small rocket motors are presented. The results presented are meant to provide the reader with an overview of the rocket motor inspection system concepts. For a detailed description of system operating and maintenance procedures, the reader is referred to the operator's manual which was supplied with the inspection system.

Figure 3.1 shows a basic overview of the Rocket Motor Inspection System in block diagram form. The system controller communicates with most of the system components digitally via the IEEE-488 interface. Many of the set up and control functions are controlled by the system controller to provide the operator with an easy to use, simple inspection procedure. The function of most of the components of this block diagram are self evident except for the analog electronics which are specific to the ultrasonic inspections being performed. These will be explained in greater detail in subsequent sections.

All of the results to be presented in the following sections were obtained using inert Sidewinder rocket motors supplied by the Rocket Propulsion Laboratory of Edwards Air Force Base. While the results presented in this section are specifically related to this one type of rocket motor, the techniques and procedures should be widely applicable to a large number of rocket motors.

3.1 DEBOND INSPECTION SYSTEM

The debond inspection procedure is based upon the chirped frequency measurement techniques described in the previous section. The technique relies upon measurement and interpretation of a "Q-signature" and "R-signature" to determine the presence or absence of a debonded layer within the rocket motor

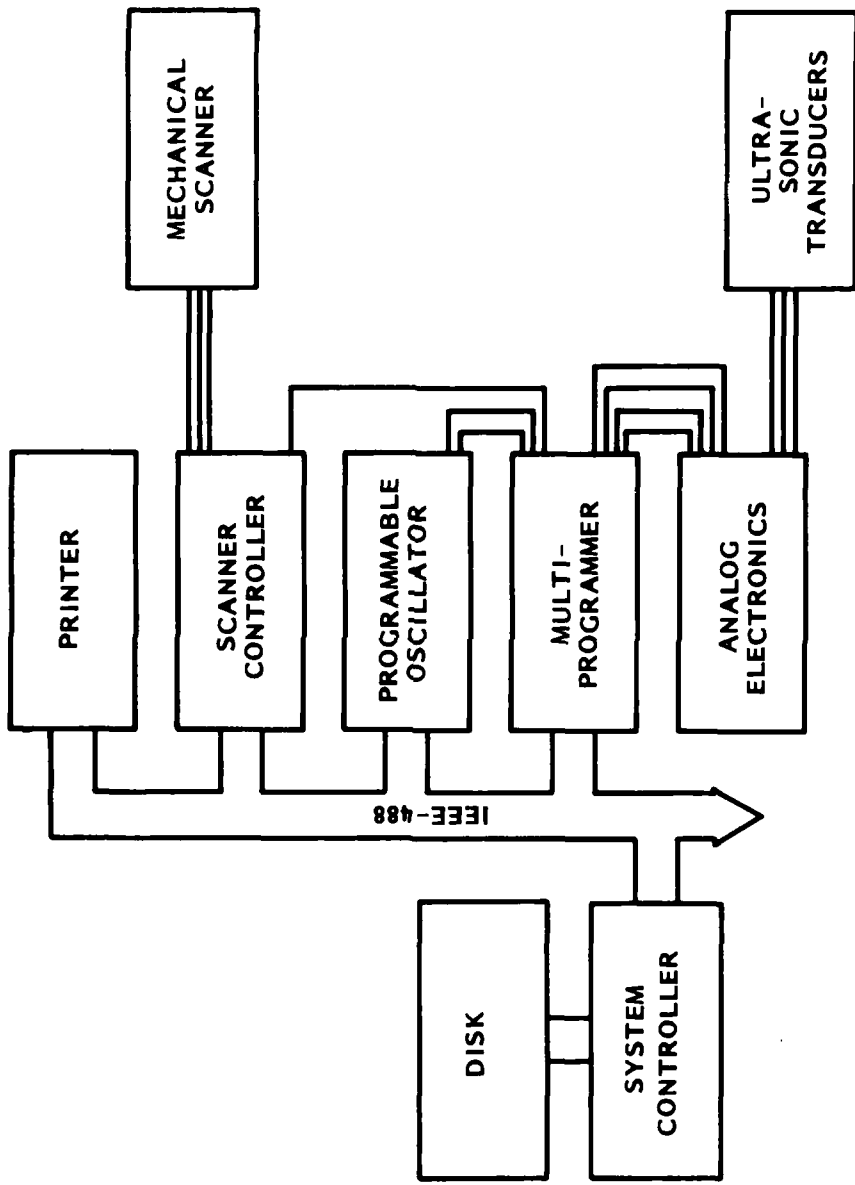


Figure 3.1 Overall block diagram of the rocket motor inspection system.

wall. Within this section of the report, the equipment used to make these measurements as well as the results of these measurements are presented.

3.1.1 Equipment Overview

Two basic subsystems make up the chirp frequency debond inspection system: 1) transducer coupling subsystem, and 2) analog electronics subsystem.

3.1.1.1 Transducer and coupling subsystem

Figure 3.2 shows the transducer and coupling subsystem used by the chirped frequency debond inspection system. The unit consists of a mechanical fixture for holding and manipulating the ultrasonic transducer and a fluid filled reservoir for coupling the ultrasonic energy into the motor wall. A means is provided for aligning the transducer so that the sound field produced will be normally incident upon the rocket motor wall. The alignment fixture was made to hold conventional 0.500 inch (12.7 mm) immersion transducers which have a nominal 0.625 inch (15.9 mm) outside diameter. The center frequency and bandwidth of the transducer used must be chosen based upon the resonant behavior of the rocket motor wall to be inspected.

A thin Teflon® membrane is used to separate the fluid reservoir from the rocket motor wall. Two small nozzles and a pressurized water system are used to provide a continuous flow of water on the rocket motor wall to maintain acoustic coupling.

3.1.1.2 Electronics subsystem

A block diagram of the electronics used to perform the chirp frequency measurements is shown in Figure 3.3. The following is a brief description of operation.



Figure 3.2 Photograph showing the debond test transducer and related mechanical assembly.

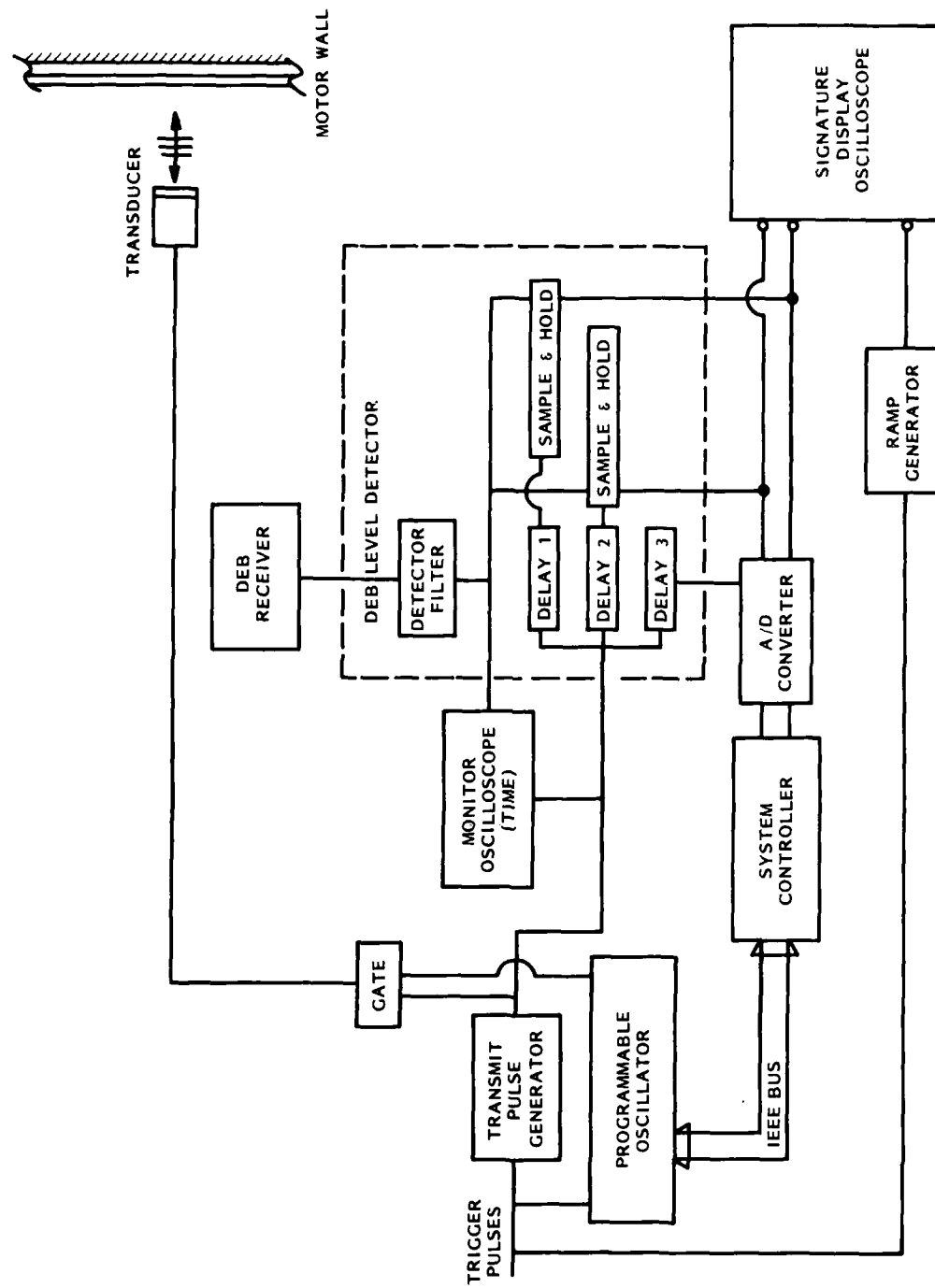


Figure 3.3 Block diagram of the analog electronics used for the debond inspection.

Trigger pulses are provided for the system by two different methods: 1) generated by the computer, or 2) generated by the stepper motor scan controller. The computer generated pulses (path not shown) are used to provide a system clock during the set up and calibration portion of the test procedure and the pulses generated by the scanner are used during the data collection process. These trigger pulses cause three different operations to be initiated. First, a train of 40 transmit enable pulses are generated. These pulses are 20 microseconds long and occur every 500 microseconds. Second, the programmable oscillator is caused to sweep from the start frequency to the stop frequency. The frequency limits, sweep mode, and output level of the oscillator are controlled by the system controller. Third, a ramp generator is triggered to provide the horizontal drive for the signature display scope. The sweep rate of the oscillator is set to coincide with the sweep rate of the ramp generator and the pulse timing sequence.

The transmitter pulses and the gate are used to provide bursts of RF energy to excite the ultrasonic transducer. The energy reflected by the rocket motor is detected by the same transducer, amplified by the DEB RECEIVER, and sent to the DEB LEVEL detector. This level detector provides RF detection and filtering of the reflected ultrasonic signal and two channels of sample and hold capabilities. Delay 1 and Delay 2 are controlled by knobs on the front panel of the module and are used to control the type of data which is being recorded and displayed; i.e., R-signature or Q-signature. A complete signature, consisting of 40 measurements of amplitude versus frequency, is generated for each input trigger pulse. The output of the DEB LEVEL DETECTOR is used to drive the signature display scope and is recorded by the system controller through A/D converters.

Figure 3.4 shows the output of the monitor display oscilloscope which is used to set and monitor the chirp frequency tests. Panel A shows the system response when ultrasonic frequency is not near resonant frequency of the layered structure. Panel B shows the response near resonance. Near resonance, the amplitude of the reflected signal is reduced and the "ring down time" of the pulse is much longer. The small marks superimposed on the detected signal indicate the position in time where the sample and hold operation takes place.

Figure 3.5 shows the output of the signature display scope for a case/liner debond condition. Panel A shows the "R-signature" recorded by sampling the detected signal at the first time marker and Panel B shows the "Q-signature" recorded by sampling the detected signal at the second time marker.

3.1.2 Case/Liner Debond Results

In order to statistically evaluate the ability of the inspection system to detect case/liner debonds, the following experiment was performed. A series of 100 Q-signatures were collected and stored from a region of inert Sidewinder containing a case/liner debond and a normal portion of the rocket motor. Figure 3.6 shows the average of these measurements. Panel A shows the average Q-signature plus and minus one standard deviation for the 100 measurements made in the case/liner debond area. Panel B shows the same type of measurement made over the normal region of rocket motor. Based on these experimental curves, it is obvious that these waveforms can be distinguished based upon amplitude or area under the curve. A decision rule based upon area under the curve was implemented and had the following performance:

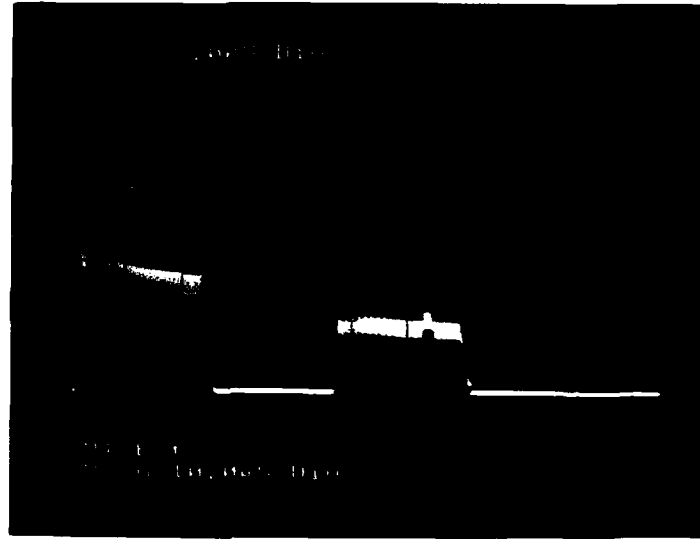


Figure 3.4A Photograph of the monitor display oscilloscope when inspection frequency is far from mechanical resonance of the rocket motor wall.

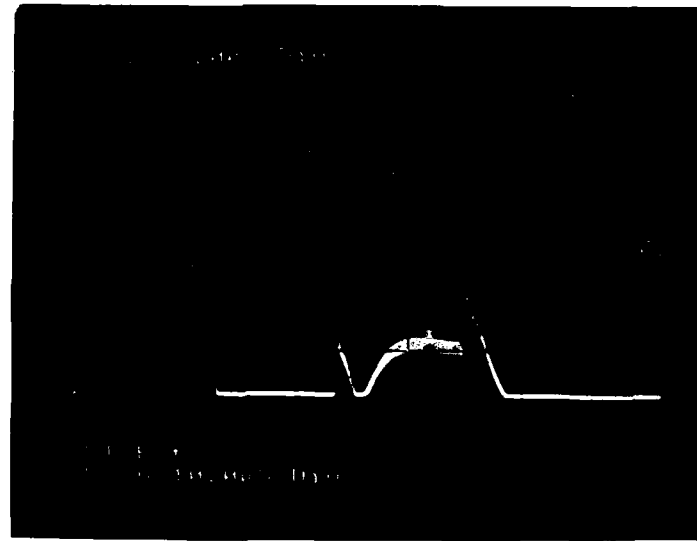


Figure 3.4B Photograph of the monitor display oscilloscope when inspection frequency is at the mechanical resonance of the rocket motor wall.

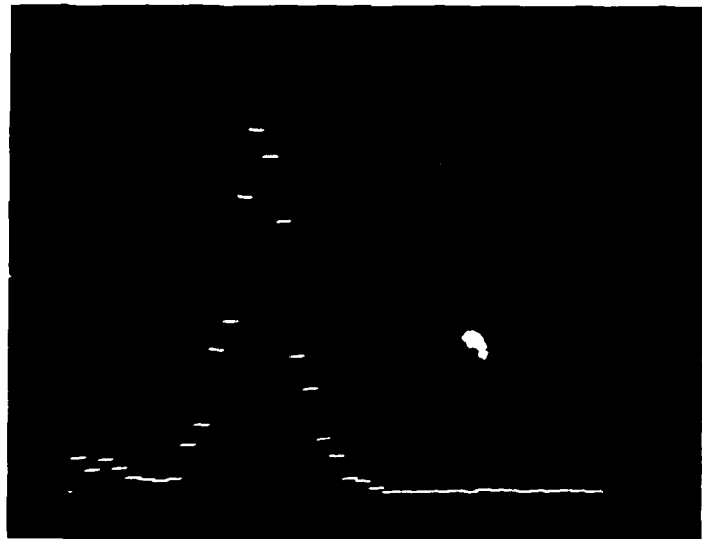


Figure 3.5A Photograph of the signature display oscilloscope showing the "Q-signature" for a Case/liner debond.

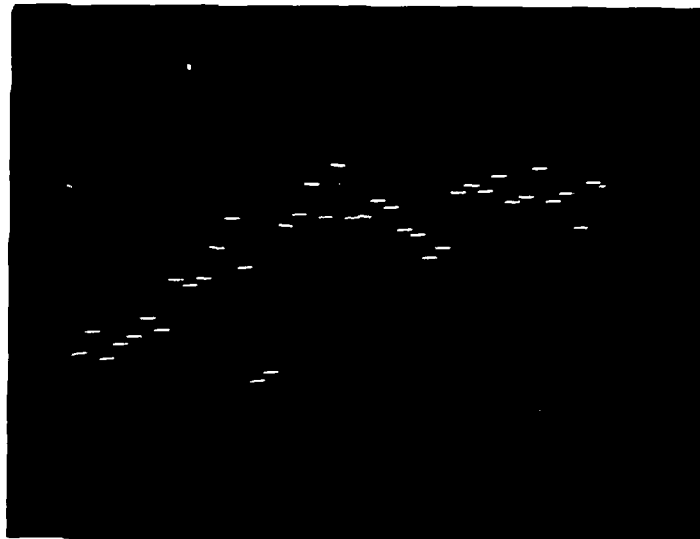


Figure 3.5B Photograph of the signature display oscilloscope showing the "R-signature" for a Case/liner debond.

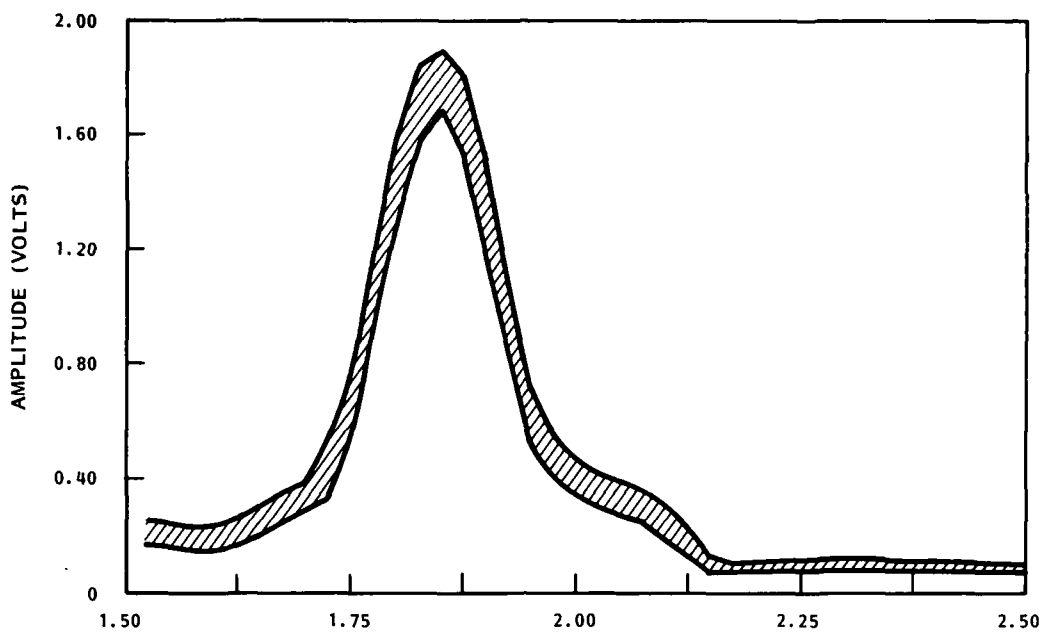


Figure 3.6A Results from a series of "Q-signature" measurements made in a region of Case/liner debond. The band represents the average, plus and minus one standard deviation, of 100 measurements.

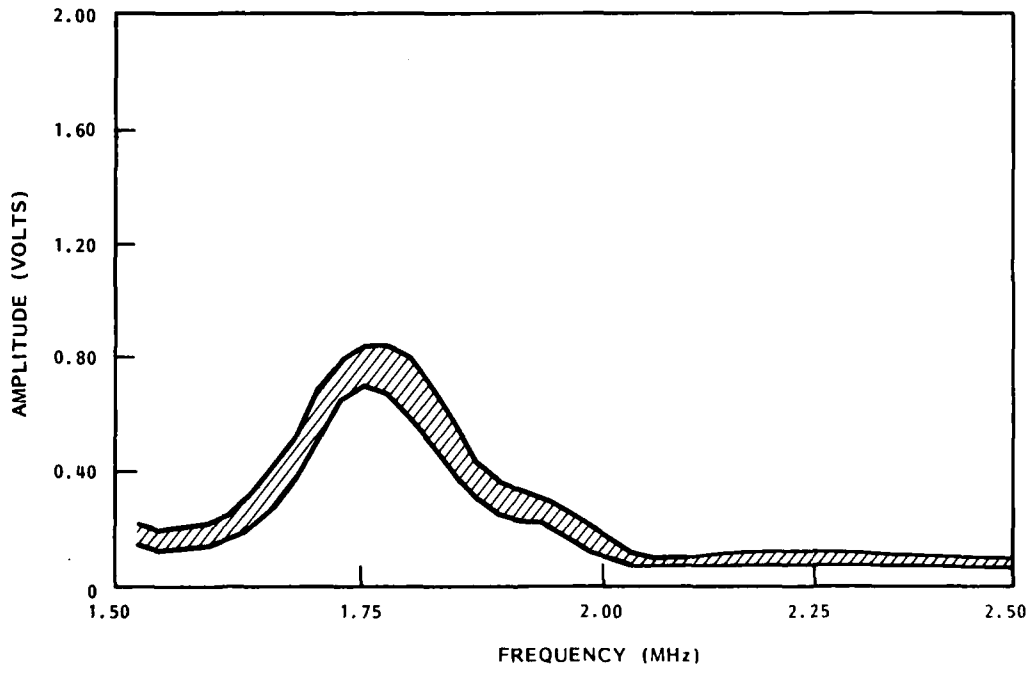


Figure 3.6B Results from a series of "Q-signature" measurements made in a Normal region. The band represents the average, plus and minus one standard deviation, of 100 measurements.

		True Class	
		Normal	Case/Liner
P R E C D L I A C S T S E D	Normal	100%	0%
	Case/Liner	0%	100%

In other words, all Q-signatures were correctly classified using the area under the curve as the distinguishing feature. In practice, the maximum of the Q-signature curve is used by the data collection system to distinguish the case/liner condition. This feature can be calculated very rapidly and has in practice been found to be quite reliable.

Figure 3.7 shows the result of a typical scan on an inert Sidewinder rocket motor in which a large area of case/liner debond was placed. The data displayed shows indicated debond regions as a function of position on the rocket motor. This data is recorded on floppy disk and can be recalled at a later time for further analysis.

3.1.3 Liner/Propellant Debond Results

A similar experiment was performed to statistically evaluate the ability of the system to detect liner/propellant debonds. Ninety-five Q-signature and R-signature waveforms were collected in the normal region of an inert Sidewinder. These data are shown in Figure 3.8 in terms of their average, plus and minus one standard deviation. A similar number of waveforms were gathered in a region of the rocket motor where a simulated liner/propellant debond was placed. These results are shown in Figure 3.9. From these two figures, it is evident that distinguishing the liner/propellant debond condition from the normal condition is very difficult. An attempt to do this was made using pattern recognition techniques.(9,10)

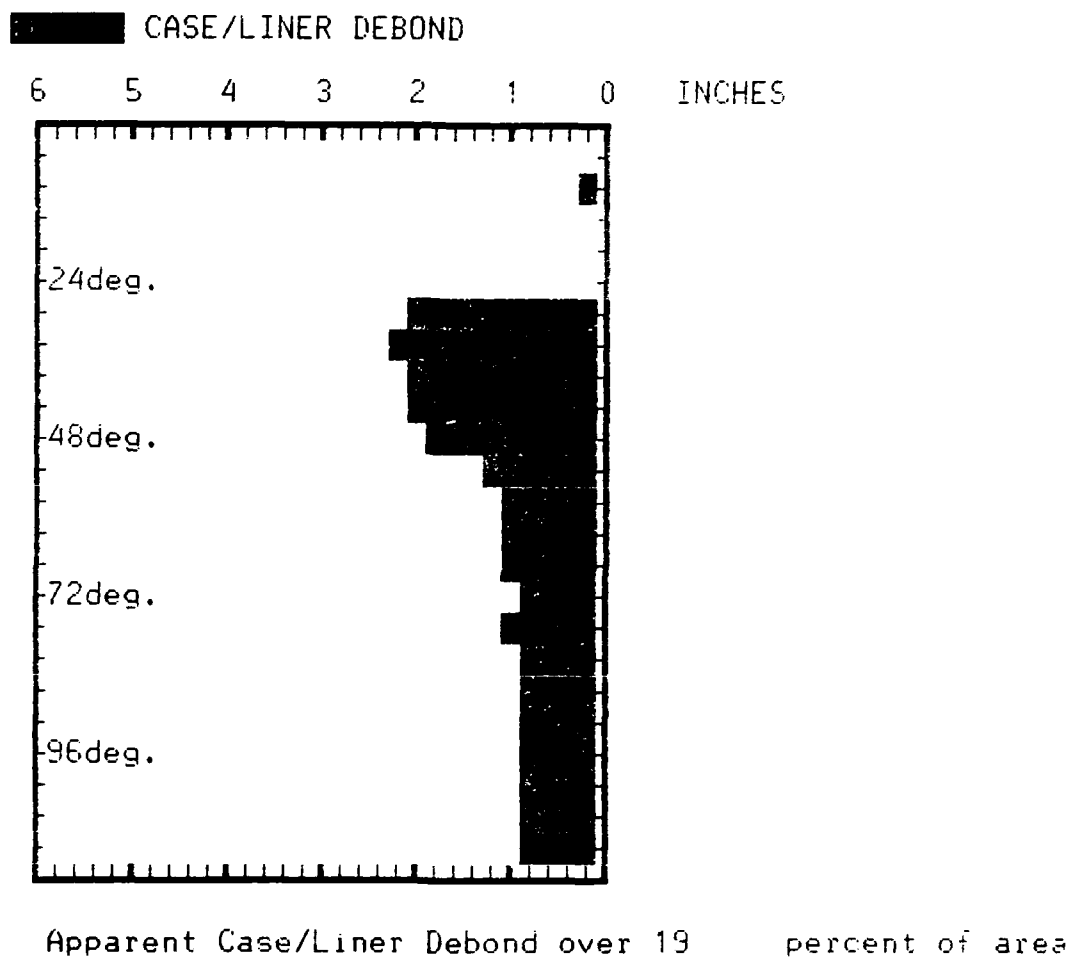


Figure 3.7 Debond defect produced by the Rocket Motor Inspection System. Dark area at the right shows an area near the end of the rocket motor where an artificial Case/Liner debond had been placed. Linear dimension represents length down the motor and the angular dimension represents rotation of the rocket motor.

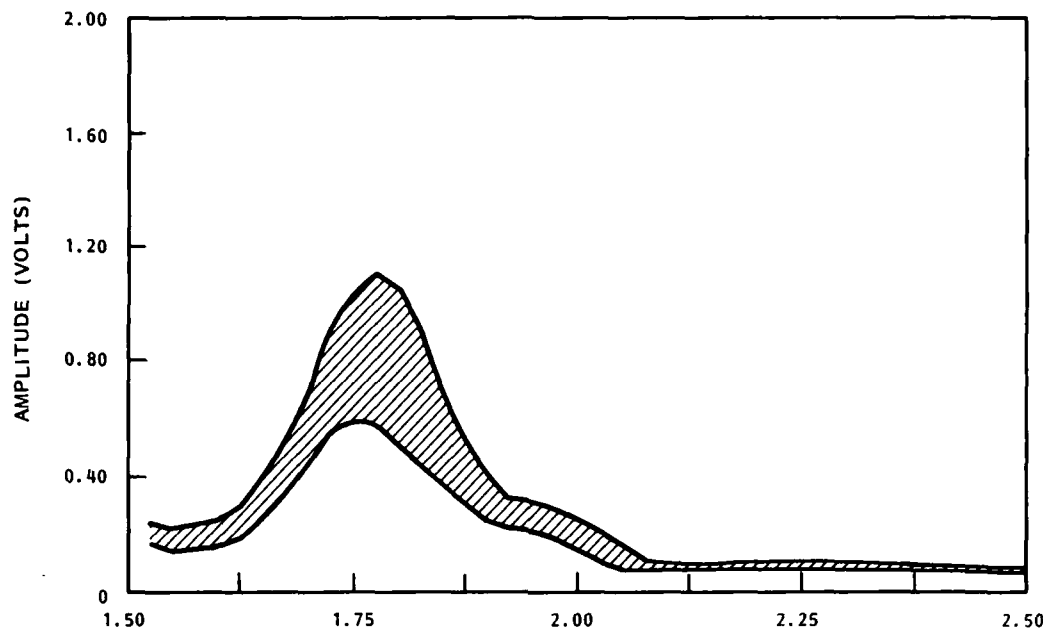


Figure 3.8A Results from a series of "Q-signature" measurements made in a region of Liner/Propellant debond. The band represents the average, plus and minus one standard deviation, of 100 measurements.

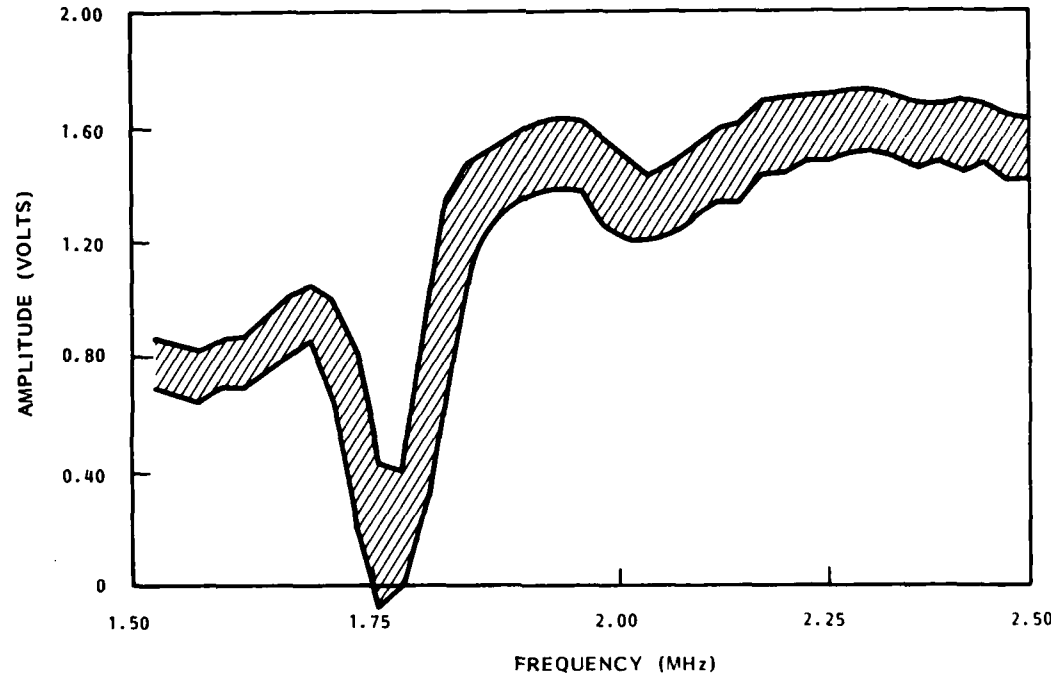


Figure 3.8B Results from a series of "R-signature" measurements made in a region of Liner/Propellant debond.

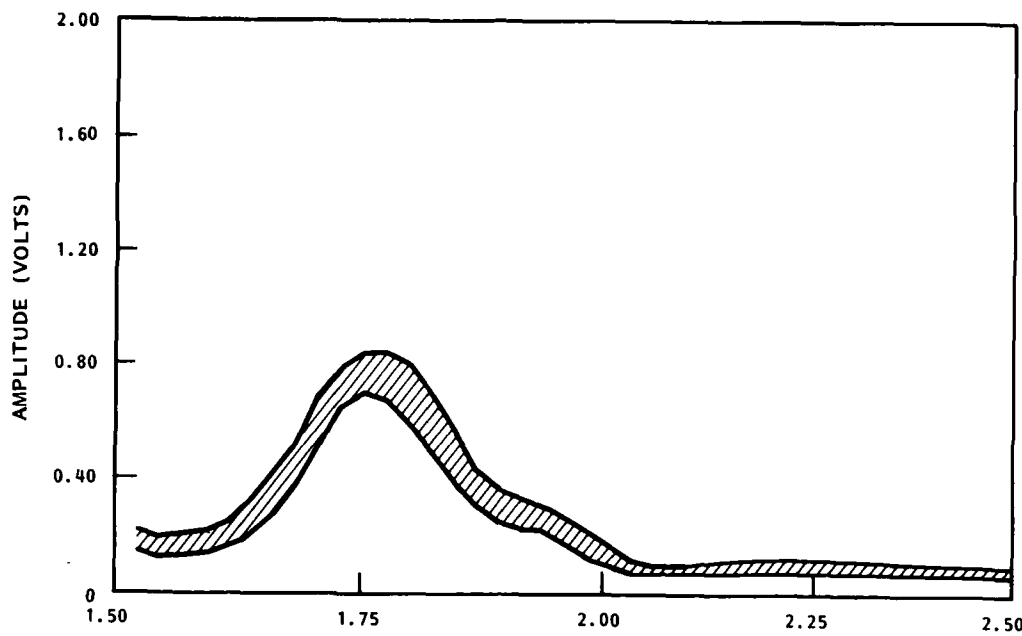


Figure 3.9A Results from a series of "Q-signature" measurements made in a Normal region. The band represents the average, plus and minus one standard deviation, of 100 measurements.

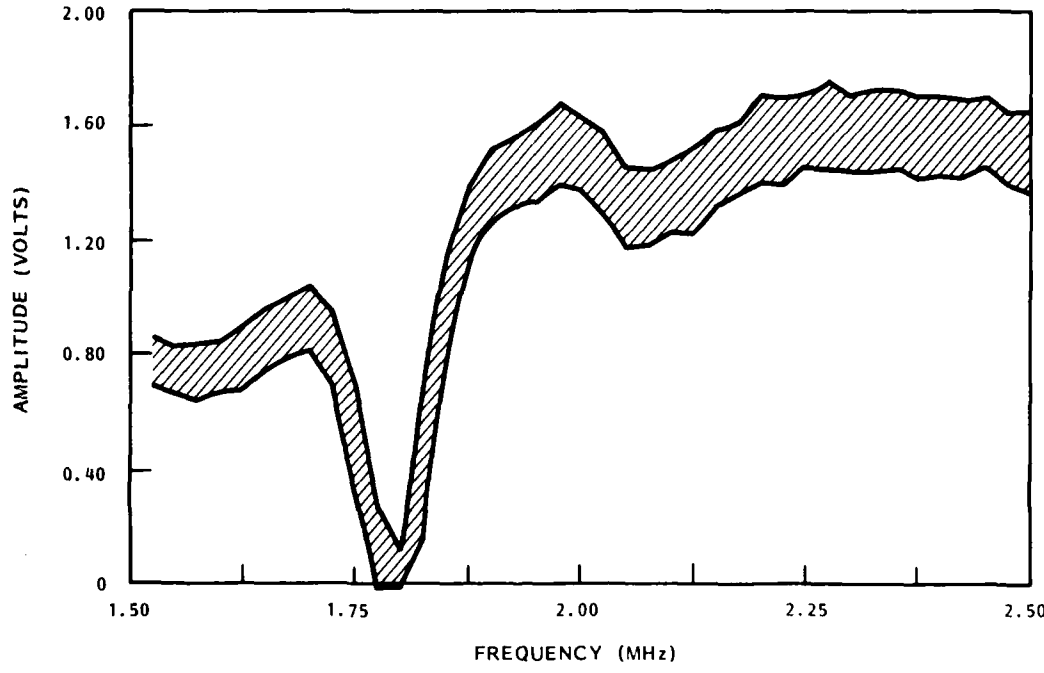


Figure 3.9B Results from a series of "R-signature" measurements made in a Normal region.

The Q-signature and R-signature curves were characterized in terms of six features:

1. frequency of peak (or dip)
2. amplitude of peak (or dip)
3. area under curve (zeroth moment)
4. ratio of first moment to second moment
5. mean squared width of curve
6. skewness of curve.

Using the Q-signature data alone, the following performance was obtained:

P	R	E C	True Class	
D	L		Normal	Liner/Propellant
I	A	Normal	80%	20%
C	S	Liner/Propellant	11%	89%
E	D			

This performance is encouraging and was obtained using only one of the features--the mean squared width of the Q-signature. In practice, however, it was found to be very difficult to reproduce these results. The decision or classification was being based upon a very minute detail of the Q-signature curve. This feature of the Q-signature curve was very strongly dependent upon the operator setup and calibration procedure.

A second attempt to analyze this data was made using the R-signature data only. This was done because there is less variability associated with this data. The data collected is not strongly affected by the operator's choice of sampling position on the time domain waveform (see Figure 3.4). The results of this analysis were as follows:

		True Class	
		Normal	Liner/Propellant
I	Normal	80%	20%
T	Liner/Propellant	45%	55%

This performance indicated that the R-signature analysis had very little predictive capability for distinguishing liner/propellant debonds from the normal rocket motor condition.

It was decided that liner/propellant debonds could only be reliably detected using the low frequency transmission test (inner bore crack test) which is discussed in the next section. Figure 3.10 shows a defect map produced on a simulated liner/propellant crack using this test. It should be noted that a single defect appears as two indications separated by approximately 80 degrees using this test. These two indications are caused first by the blocking of the transmitted beam, and second by the blocking of the reflected beam. The angular separation of these indications is determined entirely by the angular separation of the transmitting and receiving transducer.

3.2 INNER BORE CRACK INSPECTION SYSTEM

The inner bore crack test procedure is based upon a low frequency, ultrasonic transmission test. The technique uses the transmission of a narrow-band ultrasonic pulse to determine if there is any defect present in the ultrasonic path which blocks the transmission of the ultrasonic pulse. The low frequency (approximately 58 kHz) is used to provide reasonable penetration through the highly attenuating solid propellant.

||||| INNER BORE CRACK

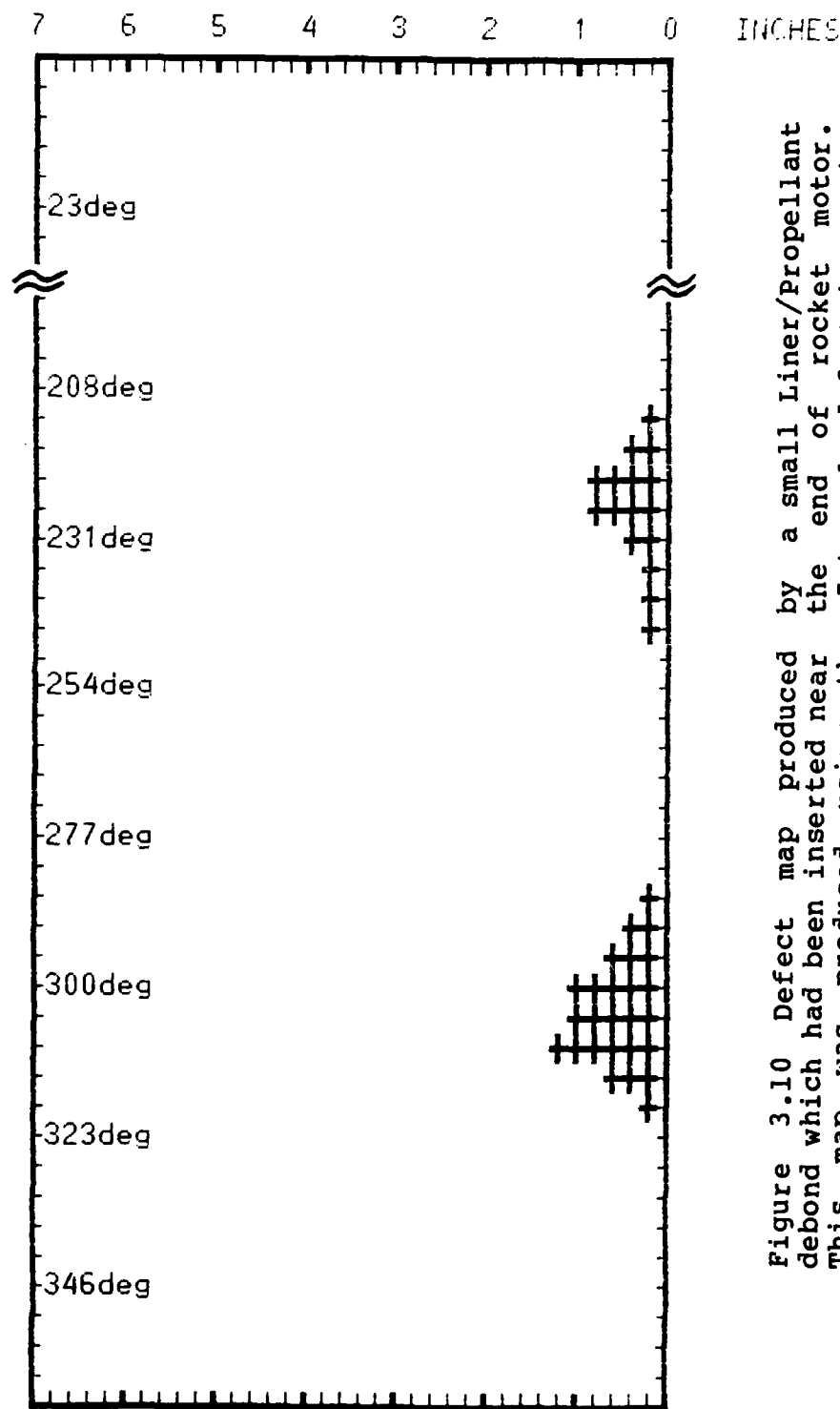


Figure 3.10 Defect map produced by a small Liner/Propellant debond which had been inserted near the end of rocket motor. This map was produced using the Internal defect inspection program.

2.16 Percent of the scanned area appears defective.

3.2.1 Equipment Overview

Two basic subsystems make up the inner bore crack inspection system: 1) the transducer and coupling subsystem, and 2) the analog electronics subsystem.

3.2.1.1 Transducer and coupling subsystem

Figure 3.11 shows the transducer and coupling subsystem used for the inner bore crack test. The unit consists of two ultrasonic transducers (marked IBC T and IBC R) and of mechanical fixtures for manipulation of each transducer. Each transducer is provided with a fluid filled reservoir for providing coupling of the ultrasonic energy into and out of the rocket motor wall. The transducers used were fabricated by Battelle and are shown schematically in Figure 3.12. The active elements are 1.5 inch (38.1 mm) diameter PZT4 discs which are 0.25 inch (6.35 mm) thick. The element is isolated from the transducer housing in an attempt to eliminate cross talk between transducers. The transducer operates in a radial mode at 58 kHz and has been fitted with a thin lens for acoustic matching and for protection of the front surface. A water coupling system is also provided for the inner bore crack transducers.

3.2.1.2 Electronics subsystem

A block diagram of the electronics used to perform the inner bore crack test is shown in Figure 3.13. The design of data collection system is very similar to that previously described for debond testing; however, the type of signal used and the detection methods differ somewhat. The following is a brief description of operation.

Trigger pulses are provided for the system by two different methods: 1) generated by the computer, or 2) generated by the stepper motor scan controller. The computer generated pulses

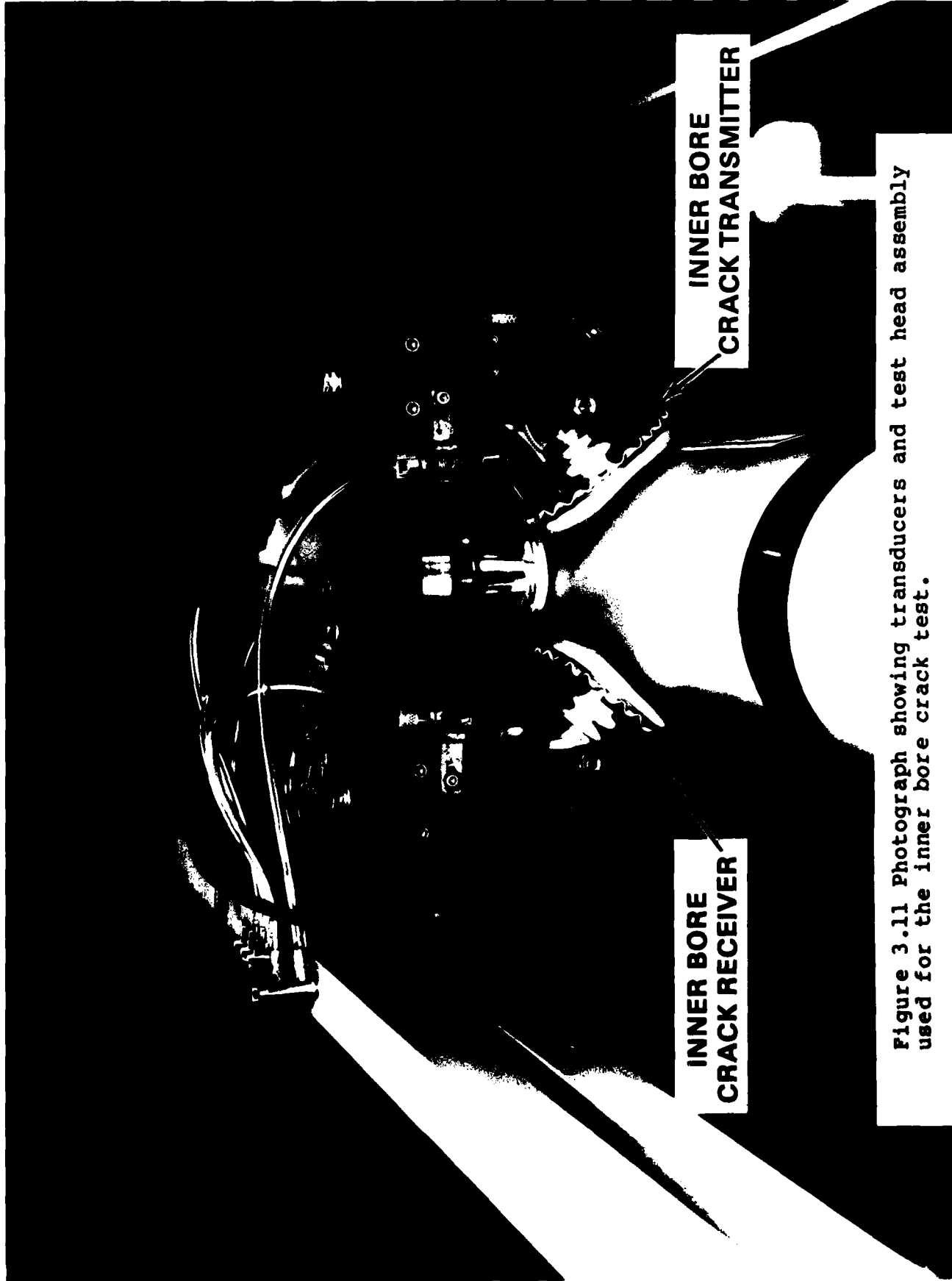


Figure 3.11 Photograph showing transducers and test head assembly used for the inner bore crack test.

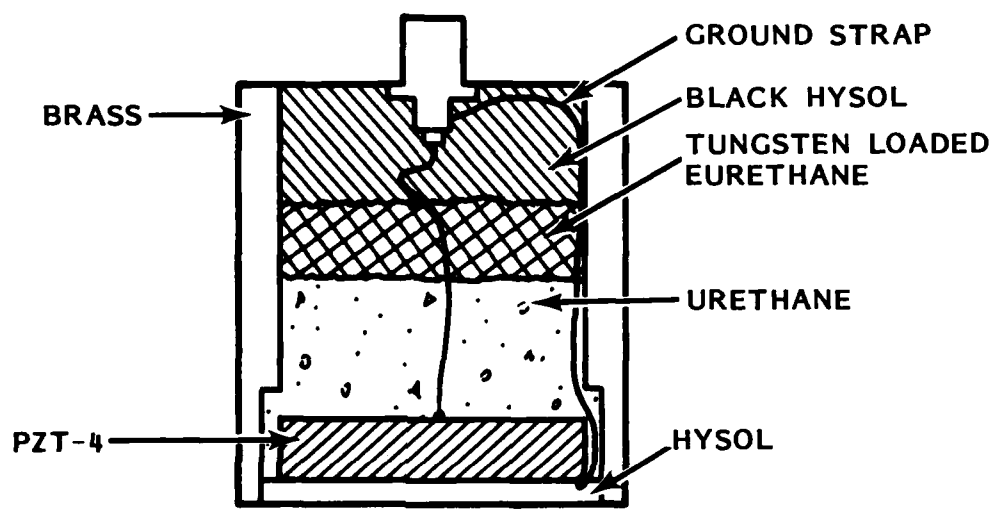


Figure 3.12 Illustration of the low frequency transducers which were fabricated to perform the inner bore crack test.

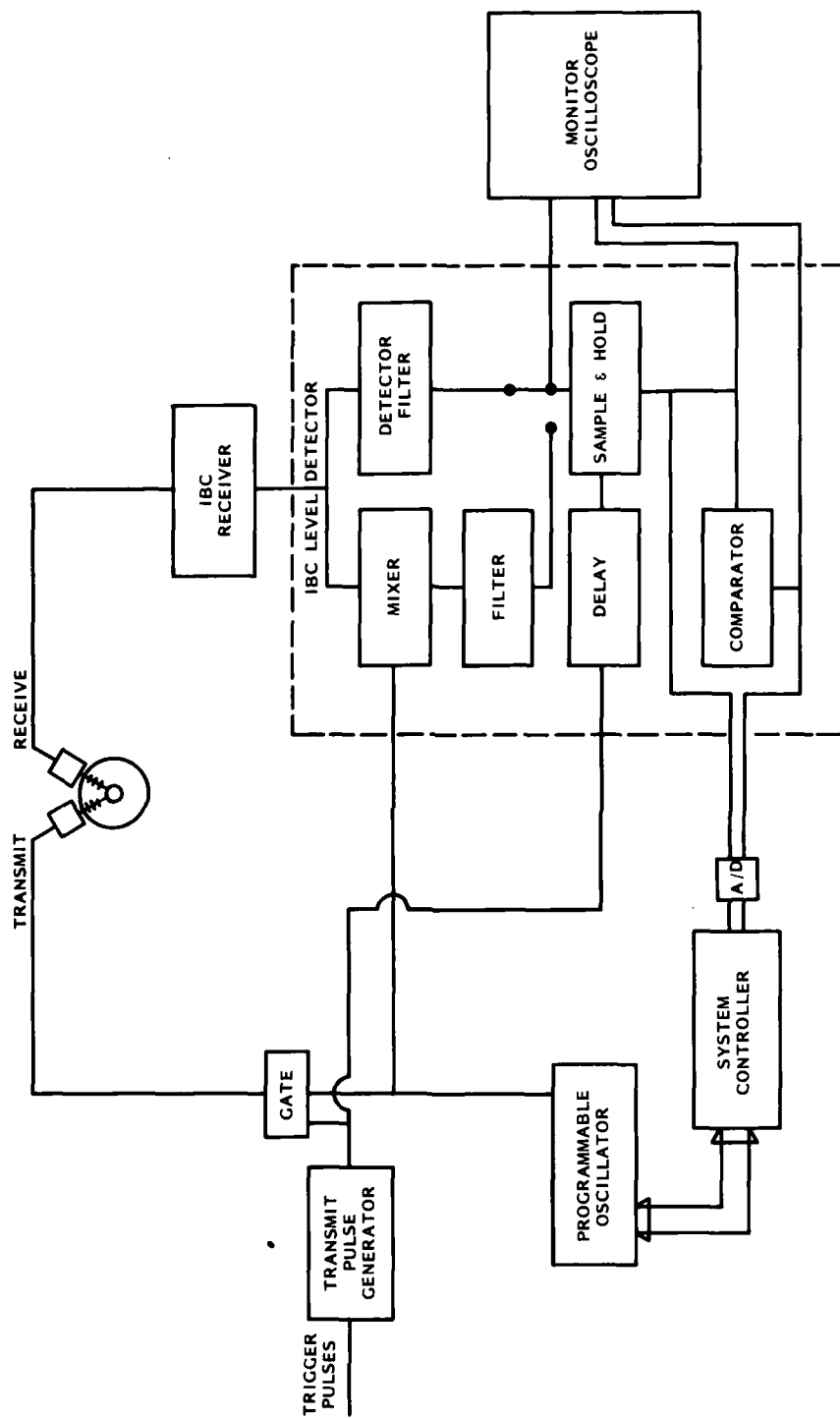


Figure 3.13 Block diagram of the electronics used for the inner bore crack test.

(path not shown) are used to provide a system clock during the setup and calibration portion of the procedure and the pulses generated by the scan controller are used during the data collection process. These trigger pulses are used to fire the transmit pulse generator. These transmit pulses and the gate are used to derive a burst of RF energy to excite the transmit transducer. The frequency and amplitude of this RF pulse are controlled by the system controller. Under normal conditions, the ultrasonic pulse propagates through the solid propellant material, is reflected by the inner bore, and is detected by the receive ultrasonic transducer. The signal is amplified by the IBC RECEIVER and passed to the IBC LEVEL DETECTOR.

Two types of detection take place within the IBC LEVEL DETECTOR: 1) conventional diode detection, and 2) phase sensitive detection. Diode detection is usually sufficient; however, phase sensitive detection was provided for use when improved signal to noise response is required. The output of either detector is sampled, held, and compared with a fixed reference voltage and is made available to the monitor oscilloscope and the A/D converter of the computer.

As an inner bore crack or internal defect blocks the transmission path of the ultrasonic energy through the rocket motor, the detected signal amplitude will drop. This drop is recorded by the system controller. If the signal falls below the specified reference voltage, an indication is recorded on the IBC defect map.

Figure 3.14 shows the output of the monitor oscilloscope. Panel A shows the system response with no defect present and Panel B shows the response with an inner bore crack blocking the transmission path. The horizontal line in each trace indicates the reference voltage which is used by the comparator for signal detection. This reference level can be manually adjusted by the operator.

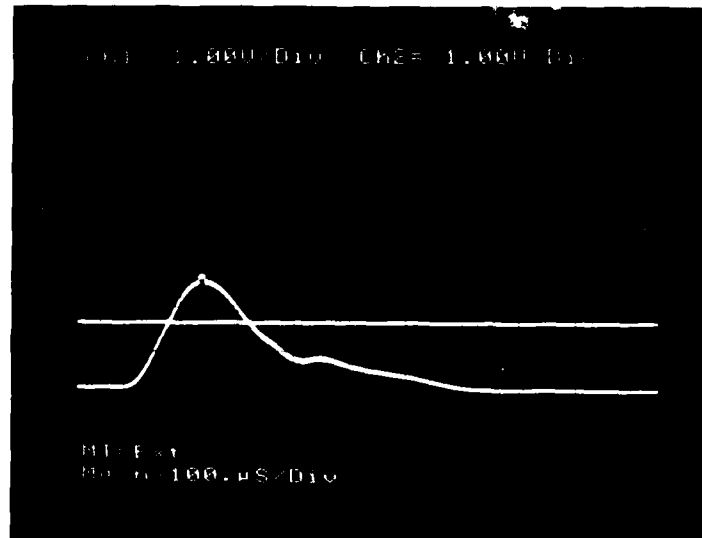


Figure 3.14A Photograph of the monitor oscilloscope showing the received signal with no defect present.

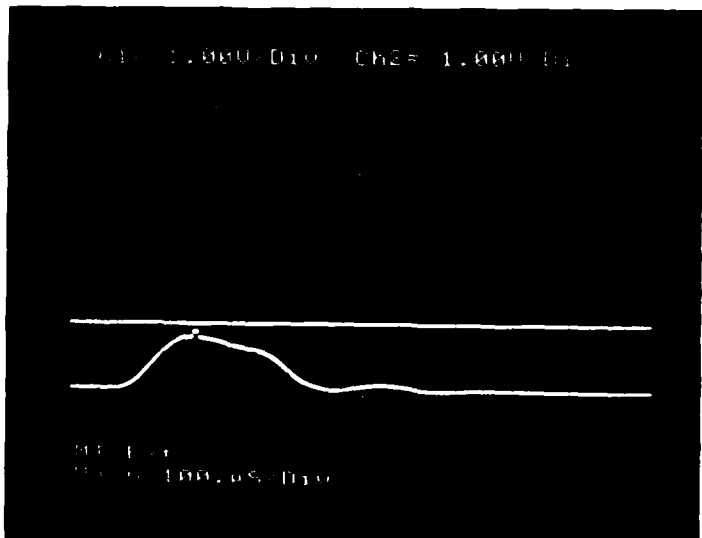


Figure 3.14B Photograph of the monitor oscilloscope showing the received signal with a defect present.

3.2.2 Inner Bore Crack Results

Figure 3.15 shows the results of mapping an inner bore crack which was present in the inert Sidewinder rocket motor. The crack, which developed over the course of this project, may have resulted from rough handling of the specimen or from period exposure of the inert propellant to water. The depth of the crack was unknown and the apparent length of crack on the inner bore of the rocket motor was 1 inch. It should be noted that defects present on the inner bore of the motor appear as a single indication using this, low frequency transmission test.

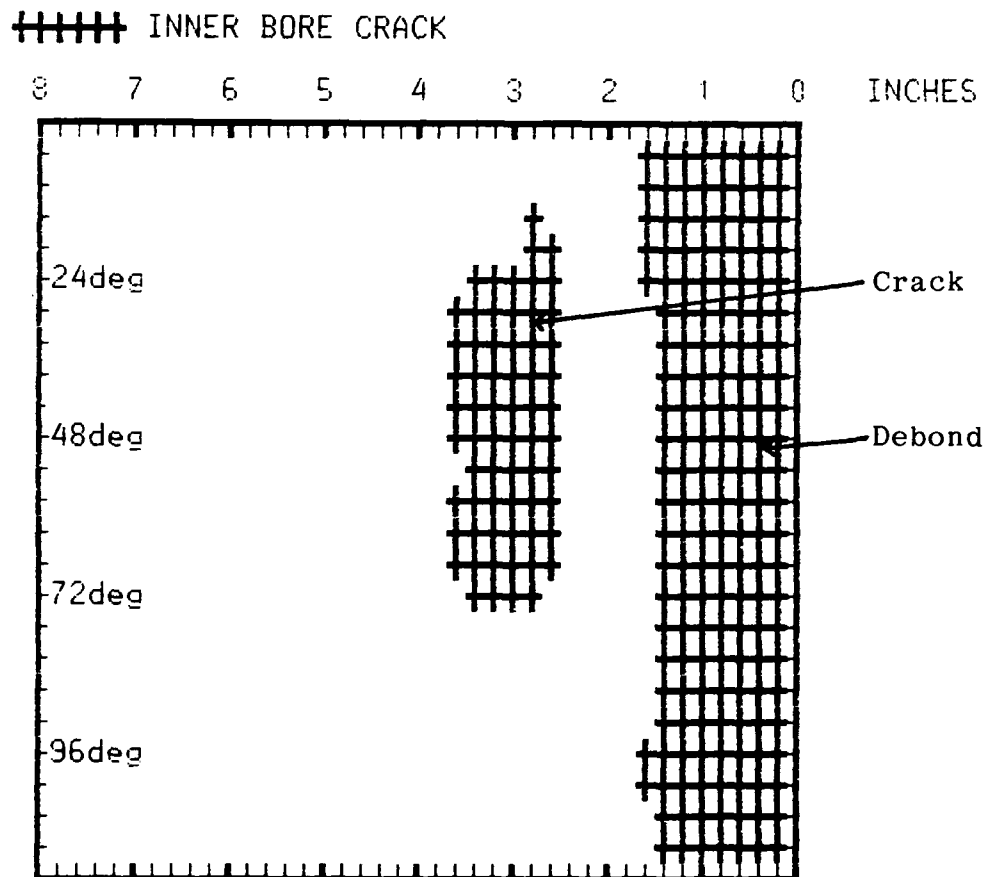


Figure 3.15 Defect map produced by a naturally occurring inner bore crack. Large area at the right of the map is an artificially induced debond region.

4.0 REFERENCES

1. Collins, H.D., "Acoustical Chirp Frequency Techniques for Debond Inspection in Solid Rocket Motor Dome Sections," Final Report - Contract No. F04611-77-C-0044, AFRPL.
2. Collins, H.D., "Diversification of Acoustical Holography as a Nondestructive Inspection Technique to Determine Aging Damage in Solid Rocket Motors," AFRPL-TR-76-37.
3. Collins, H.D., "Solid Rocket Motor Inspection by Acoustical Holography Techniques," AFRPL-TR-74-83.
4. Collins, H.D., "Acoustical Focused Holography Scanning Techniques for Imaging Inner Bore Radial Defects in Minuteman Missile Sections," paper presented at the Nondestructive Evaluation Symposium sponsored by ASNT and Southwest Research Institute, San Antonio, TX, 1975.
5. Collins, H.D., "Acoustical Chirp Frequency and Computer Correlation Technique for Debond Inspection in Solid Rocket Motor Sections," paper presented at First International Symposium on Ultrasonic Materials Characteristics, National Bureau of Standards, Gaithersburg, MD, June 7-9, 1978.
6. Collins, H.D., "Acoustical Chirp Frequency and Computer Correlation Technique for the Multi-Layer Inspection of Solid Rocket Motor Cases," paper presented at the 12th International Symposium on Nondestructive Evaluation, San Antonio, TX, April 1979.
7. Kinsler, L.E. and A.R. Frey, Fundamentals of Acoustics, Wiley, 1962, Lib. of Congress No. 62-16151.
8. Heuter, T.F. and R.H. Bolt, Sonics - Techniques for Use of Sound and Ultrasound in Engineering and Science, John Wiley and Sons, Inc., New York, 1955.

9. Harrington, T.P. and P.G. Doctor, "Data Analysis Methods for Nondestructive Evaluation," Battelle, Pacific Northwest Laboratories No. BN-SA-1056.
10. Duewer, D.L., J.R. Koskinen, and B.R. Kowalski, "ARTHUR and Experimental Data Analysis," available from the Laboratory of Chemometrics, University of Washington, Seattle, WA 98195.

END

FILMED

4-84

DTIC